Bull Volcanol (2011) 73:1583–1609
DOI 10.1007/s00445-011-0564-y

RESEARCH ARTICLE

The flow dynamics of an extremely large volume pyroclastic flow, the 2.08-Ma Cerro Galán Ignimbrite, NW Argentina, and comparison with other flow types

Ray A. F. Cas · Heather M. N. Wright · Christopher B. Folkes · Chiara Lesti · Massimiliano Porreca · Guido Giordano · Jose G. Viramonte

Received: 30 December 2010 / Accepted: 19 September 2011 / Published online: 16 November 2011

Abstract The 2.08-Ma Cerro Galán Ignimbrite (CGI) represents a >630-km^3 dense rock equivalent (VEI 8) eruption from the long-lived Cerro Galán magma system (~6 Ma). It is a crystal-rich (35–60%), pumice (<10% generally) and lithic-poor (<5% generally) rhyodacitic ignimbrite, lacking a preceding plinian fallout deposit. The CGI is preserved up to 80 km from the structural margins of the caldera, but almost certainly was deposited up to 100 km from the caldera in some places. Only one emplacement unit is preserved in proximal to medial settings and in most distal settings, suggesting constant flow conditions, but where the pyroclastic flow moved into a palaeotopography of substantial valleys and ridges, it interacted with valley walls, resulting in flow instabilities that generated multiple depositional units, often separated by pyroclastic surge deposits. The CGI preserves a widespread sub-horizontal fabric, defined by aligned elongate pumice and lithic clasts, and minerals (e.g. biotite). A sub-horizontal anisotropy of magnetic susceptibility fabric is defined by minute magnetic minerals in all localities where it has been analysed. The CGI is poor in both vent-derived ('accessory') lithics and locally derived lithics from the ground surface ('accidental') lithics. Locally derived lithics are small (<20 cm) and were not transported far from source points. All data suggest that the pyroclastic flow system producing the CGI was characterised throughout by high sedimentation rates, resulting from high particle concentration and suppressed turbulence at the depositional boundary layer, despite being a low aspect ratio ignimbrite. Based on these features, we question whether high velocity and momentum are necessary to account for extensive flow mobility. It is proposed that the CGI was deposited by a pyroclastic flow system that developed a substantial, high particle concentration granular under-flow, which flowed with suppressed turbulence. High particle concentration and fine-ash content hindered gas loss and maintained flow mobility. In order to explain the contemporaneous maintenance of high particle concentration, high sedimentation rate at the depositional boundary layer and a high level of mobility, it is also proposed

Editorial responsibility: K. Cashman

This paper constitutes part of a special issue:

Cas RAF, Cashman K (eds) The Cerro Galan Ignimbrite and Caldera: characteristics and origins of a very large volume ignimbrite and its magma system

R. A. F. Cas (✉) · H. M. N. Wright · C. B. Folkes
School of Geosciences, Monash University,
Clayton, VIC 3800, Australia
e-mail: ray.cas@monash.edu

C. Lesti · M. Porreca · G. Giordano
Dipartimento di Scienze Geologiche, Università di Roma Tre,
Lago S. Leonardo Murialdo 1,
00146 Rome, Italy

J. G. Viramonte
Instituto GEONORTE and CONICET,
Universidad Nacional de Salta,
Buenos Aires 177,
4400 Salta, Argentina

Present Address:
H. M. N. Wright
US Geological Survey,
MS 910,
Menlo Park, CA 94025, USA

Present Address:
M. Porreca
Centro de Vulcanologia e Avaliação de Riscos Geológicos (CVARG), Universidade dos Açores,
Rua Mae de Deus,
9501 Ponta Delgada, Portugal

that the flow(s) was continuously supplied at a high mass feeding rate. It is also proposed that internal gas pressure within the flow, directed downwards onto the substrate over which the flow was passing, reduced the friction between the flow and the substrate and also enhanced its mobility. The pervasive sub-horizontal fabric of aligned pumice, lithic and even biotite crystals indicates a consistent horizontal shear force existed during transport and deposition in the basal granular flow, consistent with the existence of a laminar, shearing, granular flow regime during the final stages of transport and deposition.

Keywords Cerro Galán caldera/ignimbrite · VEI 8 magnitude eruption · Crystal-rich ignimbrite · Laminar-like · Shearing · Granular flow

Introduction

Volcanological understanding of the flow, transport and depositional behaviour of pyroclastic flows has been traditionally based mainly on the study of small-to-intermediate volume flows and their deposits, especially from historic and recent events (e.g. Mount St Helens in 1980; Rowley et al. 1981; Soufriere Hills, 1995–present, Loughlin et al. 2002; Pinatubo in 1991; Scott et al. 1996; Unzen 1990–1995, Yamamoto et al. 1993; Nakada and Fujii 1993). Studies of the facies characteristics of recent and pre-historic small-to-moderate volume pyroclastic flow deposits (e.g. Hildreth 1983; Freundt and Schmincke 1986; Pittari et al. 2006), as well as experiments and modelling of pyroclastic flow behaviour (e.g. Roche et al. 2005, 2008, 2010; Dufek and Bergantz 2007; Dellino et al. 2007; Druitt et al. 2007; Dufek and Manga 2008; Dufek et al. 2009; Giordano and Dobran 1994; Valentine and Wohletz 1989; Bursik and Woods 1996), have contributed greatly to the understanding of the flow behaviour of pyroclastic flows. However, extremely large volume (≥VEI 8) pyroclastic flow forming eruptions have not occurred in historic times, and there are few studies of the detailed facies architecture of ignimbrites of this magnitude (e.g. Wilson 2001; Wilson and Hildreth 1997, 2003).

The 2.08-Ma Cerro Galán Ignimbrite (CGI) of northwestern Argentina resulted from a >630-km^3 (dense rock equivalent, DRE) explosive eruption from the long-lived Cerro Galán caldera system. Deposits are preserved radially up to 80 km from the original structural margins of the caldera (Folkes et al. 2011a). Although the original distal extent was greater before erosion, current distal outcrops preserve numerous contacts of the ignimbrite with basement and palaeotopography, which we use here, together with the facies characteristics and architecture of the ignimbrite, to infer the flow dynamics of the pyroclastic flow system, especially in distal areas.

Geological setting

The CGI was erupted from the Cerro Galán caldera (Francis et al. 1978, 1989) in the Central Volcanic Zone of the Andes continental margin volcanic arc (Stern 2004) at about 2.08 Ma (Folkes et al. 2011a; Figs. 1 and 2). The Cerro Galán topographic caldera has dimensions of 38×26 km and is elongate in a north–south direction. The original structural margins of the caldera had dimensions of 26×18 km (Folkes et al. 2011a). The caldera is located at the intersection of the northwest trending Archibarca–Galán lineament and a set of north–south trending faults known as the Diablillos–Galán Fault Zone (Viramonte et al. 1984). The CGI represents the most recent and largest volume ignimbrite erupted from the long-lived Cerro Galán magma system, which began eruptive activity at about 6 Ma, represented by the Toconquis Formation ignimbrites (Sparks et al. 1985; Folkes et al. 2011a). The distribution and stratigraphy of the Toconquis Formation indicates that repeated eruptions occurred from an antecedent Cerro Galán caldera (Folkes et al. 2011a).

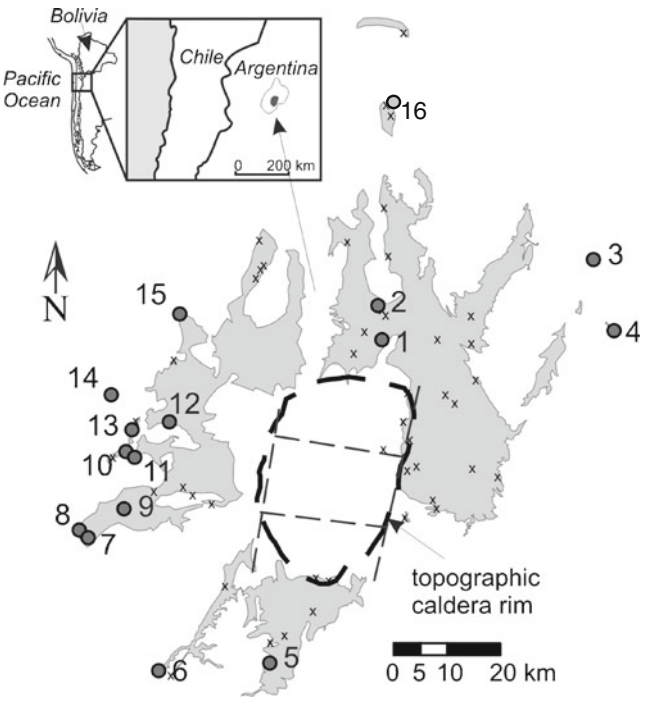

Fig. 1 Location of the Cerro Galán Caldera in northwestern Argentina, in the Central Volcanic Zone of the Andean continental margin arc system. The preserved extent of the 2.08-Ma Cerro Galán Ignimbrite (*shaded*), the locations of logged localities (x) and the locations of the sites referred to in the text (*numbered dots*) are shown. *1* Diamante, *2* Aguas Calientes, *3* Tacuil, *4* Hualfin, *5* Laguna Media, *6* El Toro, *7* Antofagasta de al Sierra, *8* Northwest of Antofagasta, *9* Las Pitas Medial, *10* Curuto, *11* Ojo de Curuto, *12* Puntas Negras, *13* Punilla, *14* Nacimientos, *15* Beltran 'run-up'. Also see Table 1 for a summary of each numbered locality

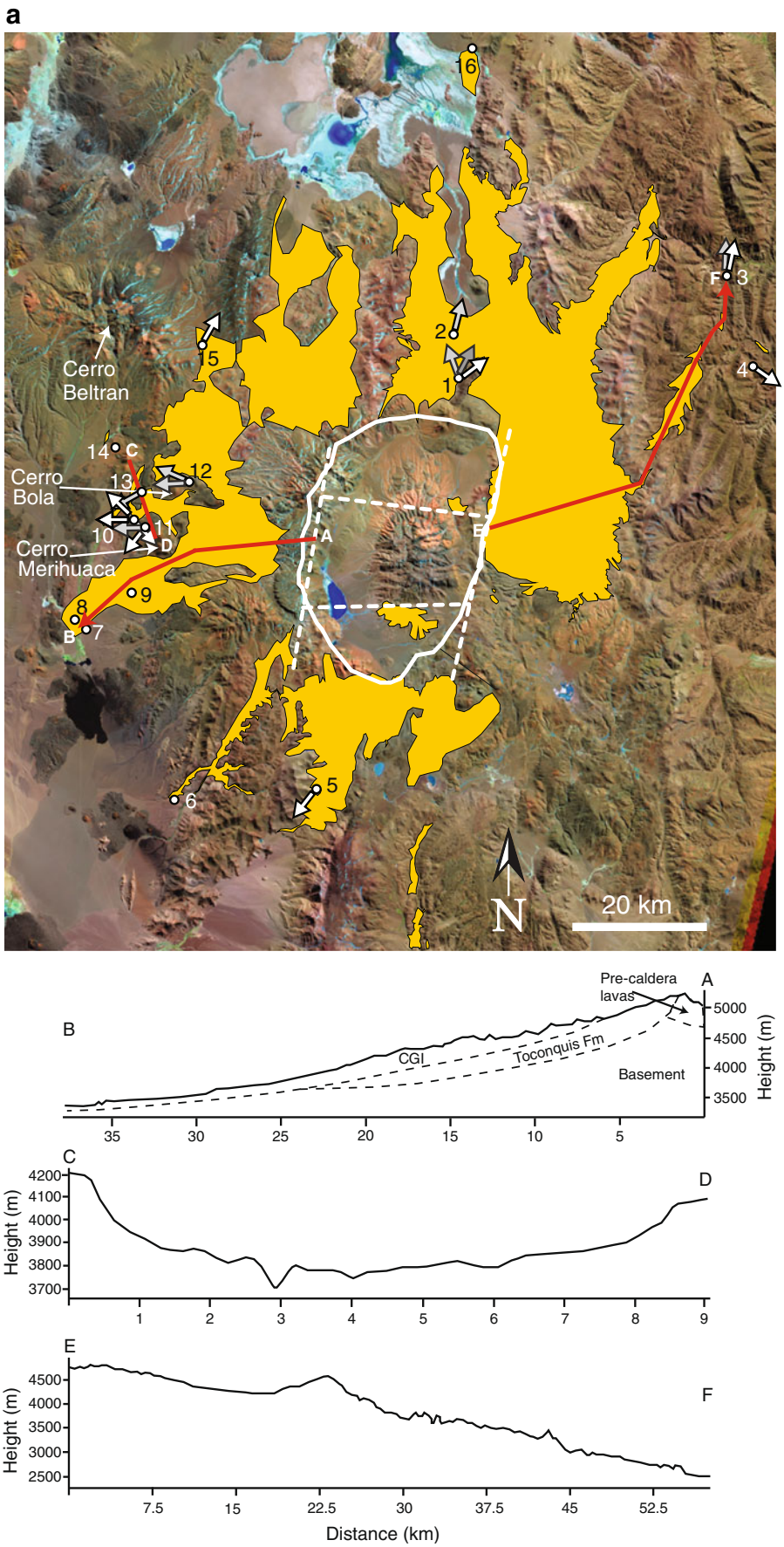

Fig. 2 **a** Distribution of Cerro Galán ignimbrite superimposed on a Landsat satellite image. *Arrows* indicate AMS flow directions; *white arrows* represent the base of the ignimbrite; *light grey arrows* correspond to middle heights; *dark grey arrows* indicate the top of the ignimbrite. Numbers represent localities discussed in the text and in Table 1. *1* Diamante, *2* Aguas Calientes, *3* Tacuil, *4* Hualfin, *5* Laguna Media, *6* El Toro, *7* Antofagasta de al Sierra, *8* Northwest of Antofagasta, *9* Las Pitas Medial, *10* Curuto, *11* Ojo de Curuto, *12* Puntas Negras, *13* Punilla, *14* Nacimientos, *15* Beltran 'run-up', *16* Fulgurite yardangs. Topographic profiles *A–B* and *E–F* are radial to the caldera, giving an indication of the palaeoslope the pyroclastic flow traversed, whereas section *C–D* provides perspective on palaeovalley relief in basement rocks west of the caldera, which has been re-excavated since being partly filled by the CGI. **b** Sloping Cerro Galán Ignimbrite shield/sheet surface north of Curuto (locality 10)

Fig. 2 (continued)

Methods

The preserved CGI extent was recorded using a combination of field mapping and analysis of Landsat images. At selected localities, vertical graphic logs were measured to document in detail the deposit characteristics, including preserved thickness, number of depositional units, depositional structures, deposit texture, component abundance of pumice, lithic clasts, crystal content and matrix content using visual estimation charts and component types (pumice, lithic and crystal types). Samples were collected for geochronology (Folkes et al. 2011a), geochemistry (Folkes et al. 2011b), component analysis (e.g. Wright et al. 2011a) and palaeomagnetic analysis (Lesti et al. 2011).

In addition, we have undertaken analysis of flow directions by collecting orientated cores in the field and using anisotropy of magnetic susceptibility (AMS) techniques (Lesti 2010). AMS data were collected from samples of the CGI matrix, to infer magnetic fabric and pyroclastic flow directions. We attribute 30% of the fabric to ferromagnetic minerals such as minute magnetic minerals less than 1 mm in length and 70% to paramagnetic biotite. As the magnetic fabric is dependent on the shape or the crystallographic directions of the magnetic (both ferromagnetic and paramagnetic) minerals, the susceptibility is described by a second rank symmetric tensor and represented by an ellipsoid where the principal axes are $K_{max}>K_{int}>K_{min}$. The plane defined by K_{max} and K_{int} and perpendicular to K_{int} is the magnetic foliation ($F=K_{int}/K_{min}$), while the K_{max} lies along the magnetic lineation ($L=K_{max}/K_{int}$). The AMS ellipsoid is also described by a series of parameters that define the anisotropy degree ($P=K_{max}/K_{min}$) and its shape (e.g. oblate or prolate shape).

In a pyroclastic flow deposit, the anisotropy and shape of AMS ellipsoids are strongly influenced by the orientation of the magnetic grains during the flow (Ort et al. 2003 and references therein). The orientation of the foliation plane with respect to the lineation and the palaeotopography is interpreted as physical imbrication of magnetic minerals in the flow and can be used to infer the flow direction. We comprehensively sampled 35 sites (403 measured samples) distributed at different distances and azimuth from the caldera and at different stratigraphic heights, from palaeovalley pond to palaeoridge top facies. Here we present only the results of 17 sites distributed in nine of the studied localities. A more comprehensive consideration of all AMS results is in preparation.

The AMS was measured by a KLY-3 kappabridge at the Paleomagnetic Laboratory at Roma Tre University, Italy. The results are represented on an equal area projection (lower hemisphere) using the Jelinek (1978) statistics and the AGICO ANISOFT software (v. 4.2, Chadima and Jelinek 2009). Here we state only the results for the particular localities summarised here (see Table 2) and use them to constrain understanding of flow behaviour. The essential data will be presented below, and more detailed data, interpretation and discussion can be found in Lesti (2010) and will be presented in a future paper.

Characteristics of the CGI and relationships to palaeotopography in distal locations

The Cerro Galán Ignimbrite (Table 1) has been dated at 2.08 Ma using sanidine $^{40}Ar/^{39}Ar$ dating (Kay et al. 2011) and also at 2.56 Ma using biotite $^{40}Ar/^{39}Ar$, as discussed by Folkes et al. (2011a). The revised stratigraphy, distribution, volume estimates and geochemistry have been re-evaluated in this special issue by Folkes et al. (2011a, b). The CGI is rhyodacitic (68.5–71 wt.% SiO_2) with a mineral assemblage consisting of, in order of decreasing abundance, plagioclase>biotite>quartz>apatite>magnetite>ilmenite>zircon>titanite>monazite. The eruptive volume of the CGI has recently been estimated at ~630 km^3 DRE (see Folkes et al. 2011a for calculation method), based on current preserved volume, estimated volume removed by erosion and crystal concentration studies to estimate volume of lost elutriated fine ash. No distal co-ignimbrite ash has yet been identified. This new volume calculation is approximately two thirds of the original DRE volume estimated by Francis et al. (1983) and Sparks et al. (1985). The CGI currently outcrops to maximum distances of 40 to ~80 km radially from the structural caldera margins (Fig. 2). In proximal to medial settings, the ignimbrite consists of one depositional unit that can be up to 80 m thick in outcrop and forms a continuous sheet (Fig. 2a, b).

In proximal localities along the western caldera topographic rim, the CGI is thinner (up to 20 m thick) and is distinctly fine-grained, whereas in distal settings, the CGI is up to 60 m thick (e.g. at locality 3, Tacuil, ~50 km from the caldera structural margins; see Figs. 2 an 3 for locality numbers related to Table 1 location names and text below) and may consist of

Table 1 Summary of location details and deposit characteristics at principal sections measured through the Cerro Galán Ignimbrite in this study

	Locality	Latitude *X*	Longitude *Y*	Direction relative from caldera	Distance from topographic rim (km)	Distance from structural rim (km)[a]	Palaeotopographic context	Number of depositional units	Deposit Thickness (m)	Main lithic types	Lithic concentration zones?	Sub-horizontal fabric?	Defining features of depositional unit boundaries	Palaeovalley axis orientation	Inferred sense of the flow by AMS data[b]
1	Diamante	0714340	7153982	N	7	19	Valley margin	1	43	PPD, FMS, MD	–	Strong lithics and pumice	–	S–N	N51°; N354°; N27°
2	Aguas Calientes	0711705	7156300	N	12	25	Valley pond	1	58	PPD, Gneiss, AMP	–	–	–	S–N	N14°
3	Tacuil	0753770	7169052	NE	43	50 (57)	Valley pond (except basal unit)	6	57	FMS, PPD	–	Strong lithics, pumice and matrix biotite crystals	Surge deposits at base of lower 4 units. Abrupt change in grain size, component change and parting between upper units	W–E (intersects a N–S valley also)	N13°; N2°
4	*N* of Hualfin	0757655	7155688	NE	40	46 (52)	Valley pond	3	55	G, PPD	–	Weak lithics and pumice	Ash layer at base of lower unit, surge deposits at base of upper 2 units	NW–SE	N125°
5	Laguna Media	0693157	7093244	SSW	18	27	Valley margin	1	20	MD, MVO, PPD	Top PPD	Lithics	–	NE–SW	N230°
6	El Toro	0672348	7091805	SW	33	36	Valley pond	1	25	MS, QBS, PPD	Base schists and metasedimentaries	Lithics	–	NE–SW	–
7	Antofagasta de la Sierra	0659134	7116844	W	32	36 (38)	Valley pond	1	14	FMS, MVO, PPD	Base schists and PPD	–	–	E–W	–
8	NW of Antofagasta de la Sierra	0657459	7118286	W	34	38 (40)	Valley margin	1	40	FMS, PPD, MVO	Basal 10-m schists and PPD	Lithics	–	E–W	–
9	Las Pitas Medial	0676765	7126380	W	25	29 (30)	Valley pond	2	19	PPD, FMS, MD	–	Weak pumice and lithics	A pumice concentration at the top of basal unit, erosional contact and discontinuous surge at the base of upper unit	E–W	–
10	Curuto	0666225	7133051	W	25	30	Valley pond and margin	1	Tapers to 0	FMS, MS, PPD	Valley margin schists, metasedimentaries	Strong pumice and lithics		E–W	N313°; N270°; N138°
11	Ojo de Curuto	0667870	7131960	W	24	28	Valley pond and margin	1	40	PPD, BA	–	Pumice and lithics	–	NE–SW	N220°; N268°
12	Puntas Negras	0674362	7138651	WNW	18	23	Valley pond	3	35		–	Weak pumice	Surge deposits at base of upper 2 units	E–W	N294°; N267°
13	Punilla	0667350	7137156	WNW	25	30	Valley pond	1	17	PPD, MVO, BA	Base schists and BA lavas	–	–	NNE–SSW	N242°

Table 1 (continued)

Locality	Latitude *X*	Longitude *Y*	Direction relative from caldera	Distance from topographic rim (km)	Distance from structural rim (km)[a]	Palaeotopographic context	Number of depositional units	Deposit Thickness (m)	Main lithic types	Lithic concentration zones?	Sub-horizontal fabric?	Defining features of depositional unit boundaries	Palaeovalley axis orientation	Inferred sense of the flow by AMS data[b]
14 Nacimientos	0663447	7143733	WNW	30	35	Valley pond	1	35	PPD, MVO, BA	–	Lithics and matrix biotite crystals	–	S–N	–
15 Beltran run-up	0676305	7158830	NW	26	31	Valley margin	1	7	PPD, BA	–	–	–	SE–NW	N32°
16 Fulgurite yardangs	0715155	7198217	N	50	64	Valley pond	1	20	PPD, FMS, QBS	–	Biotite crystals	–	S–N	–

See Figs. 2 and 3 and Table 2 and the text for more details on each locality

PPD plagioclase–phyric dacite, *MVO* meta-volcanic Ordovician, *BA* basaltic andesite (lava or dome), *MD* microdiorite, *Amp* amphibolite, *MS* mica schist, *FMS* fine mica schist, *QBS* quartz biotite schist

[a] Distances in parentheses are the calculated based on the inferred CGI runout distances in these localities (see Fig. 2)

[b] AMS data from Lesti et al. (2011)

Fig. 3 Summary graphic logs for localities discussed in the text. **a** ▶ Localities 1–8. **b** Localities 9–16. Also see Table 1 for a summary of each locality and Figs 1 and 2 for the location of each relative to the caldera

multiple depositional units (up to six at Tacuil), separated by thin, low angle cross-stratified deposits ranging from 3 to 25 cm thick, or sharp variations in proportions and sizes of lithics, pumice clasts and matrix crystals. Its original top surface has been eroded in all localities, however, so these thicknesses represent a minimum original thickness. Given its thickness in distal localities, the CGI would have certainly extended beyond the current distal outcrops. Preserved outcrops in distal areas are often in palaeovalleys, where the ignimbrite has a flat top that probably approximates the original deposit top within several metres. The CGI contains no known coarse, proximal lithic breccias (e.g. lag breccias, lithic ground layers), or any underlying fall deposits.

The CGI is a poorly sorted, pumice and lithic-poor, crystal-rich matrix-supported ignimbrite (Figs. 4 and 5). Lapilli to bomb-sized pumice clasts constitute up to 10 vol.% of the ignimbrite, with crystals constituting up to 55% of pumice clasts on a vesicle-free basis. Ash matrix, including crystal fragments, constitutes >80% of the ignimbrite. Large quartz, plagioclase, sanidine and biotite crystals account for up to 65% of the matrix, although more commonly between 40% and 50%, with the rest consisting of vitric ash, including pumice shreds and glass shards (Fig. 4b; Folkes et al. 2011a). The difference in the crystal content of the pumice clasts and the ash matrix indicates very low levels of fine vitric ash loss during the eruption and pyroclastic flow transport (maximum ~ 20–30%; Folkes et al. 2011a). Lithic clasts generally represent <3 vol.% of the ignimbrite. No gas-escape pipes have been found anywhere in the CGI, with the possible exception of Paycuqui, near Curuto (locality 10).

Lithic clasts consist mostly of schists, gneisses and amphibolites of the Neoproterozoic Pachamama and Rio Blanco Complex, Ordovician granites to granodiorites or Miocene Tebenquicho Formation andesite–dacites (Hongn and Seggiaro 2001). To the north of the volcano, the dominant sub-ignimbritic exposures are igneous–metamorphic basement with minor Tertiary volcanics. To the east and south of the volcano, the basement is also dominated by igneous–metamorphic basement. In contrast, to the west of Galán, basement outcrops are dominantly Ordovician metasedimentary and Tertiary volcanic rocks. Where lithic clasts are relatively abundant, they appear to be local, basement-derived 'accidental' lithics from subjacent or nearby basement outcrops. Cognate lithic clasts are uncommon, but porphyritic plagioclase phyric dacite lithic clasts, which occur in all outcrops of the ignimbrite, are considered to be 'accessory' or vent wall derived because no regionally widespread units of this type of dacite are known; they represent a very small component of the deposit (~1–2%).

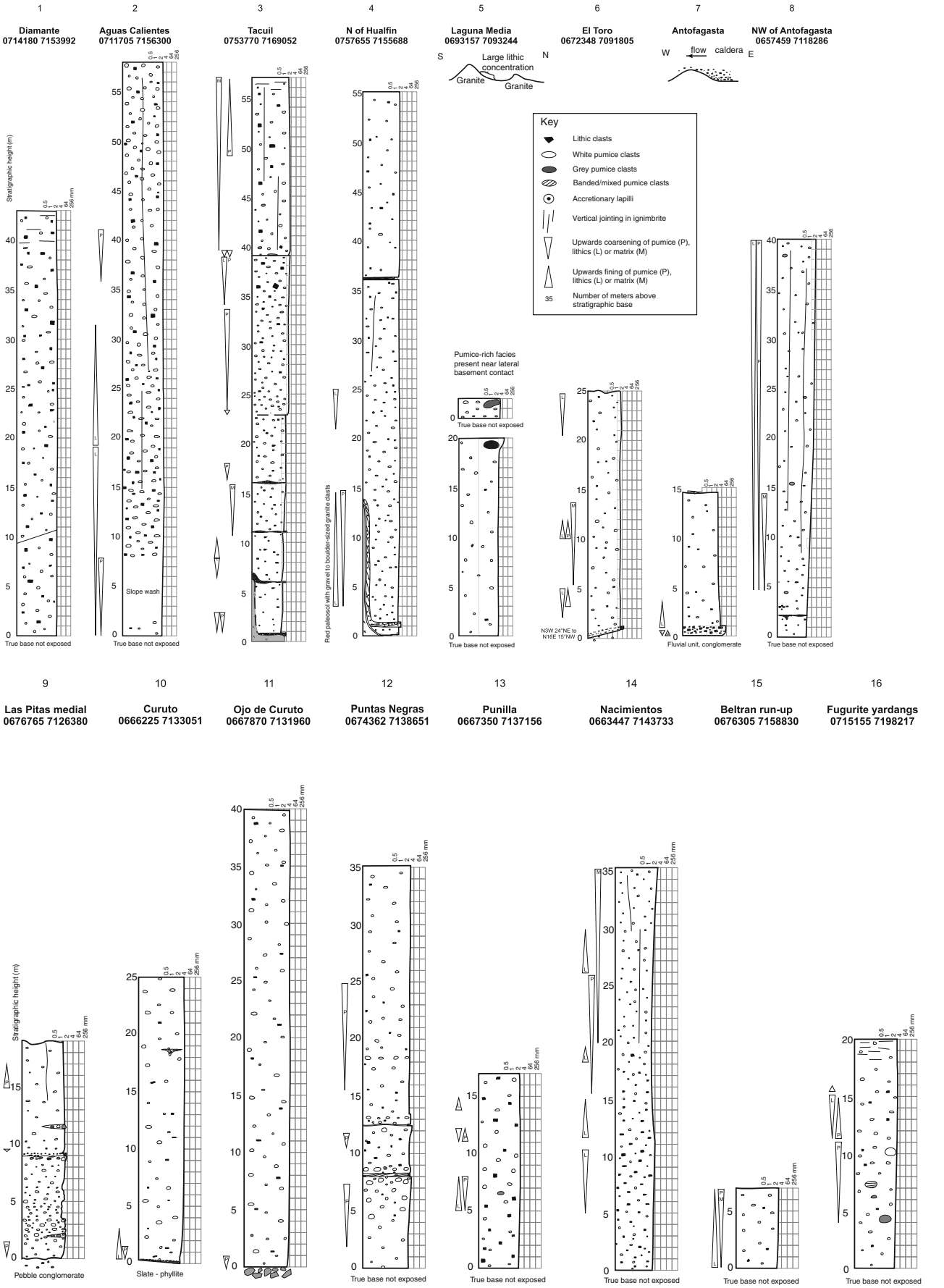
1
Diamante
0714180 7153992
2
Aguas Calientes
0711705 7156300
3
Tacuil
0753770 7169052
4
N of Hualfin
0757655 7155688
5
Laguna Media
0693157 7093244
6
El Toro
0672348 7091805
7
Antofagasta
8
NW of Antofagasta
0657459 7118286
S
N
Large lithic concentration
Granite
Granite
W
flow
caldera
E
Key
Lithic clasts
White pumice clasts
Grey pumice clasts
Banded/mixed pumice clasts
Accretionary lapilli
Vertical jointing in ignimbrite
Upwards coarsening of pumice (P), lithics (L) or matrix (M)
Upwards fining of pumice (P), lithics (L) or matrix (M)
35
Number of meters above stratigraphic base
Stratigraphic height (m)
True base not exposed
Slope wash
True base not exposed
Red paleosol with gravel to boulder-sized granite clasts
Pumice-rich facies present near lateral basement contact
True base not exposed
True base not exposed
N3W 24°NE to N16E 15°NW
Fluvial unit, conglomerate
True base not exposed
9
Las Pitas medial
0676765 7126380
10
Curuto
0666225 7133051
11
Ojo de Curuto
0667870 7131960
12
Puntas Negras
0674362 7138651
13
Punilla
0667350 7137156
14
Nacimientos
0663447 7143733
15
Beltran run-up
0676305 7158830
16
Fugurite yardangs
0715155 7198217
Stratigraphic height (m)
Pebble conglomerate
Slate - phyllite
True base not exposed
True base not exposed
True base not exposed
True base not exposed
True base not exposed

The CGI is generally moderately indurated and not amenable to sieving. It is moderately welded only in some proximal localities (Fig. 4a; welding ranks 3–4 of Quane and Russell 2005), up to 15 km to the north and east and 10 km to the south of the structural rim of the caldera. In contrast, to the west of the caldera and in all distal localities, it is non-welded (e.g. Figs. 4c and 5d), but lithified almost everywhere through vapour phase alteration (Wright et al. 2011b). Even where the ignimbrite is non-welded, it often has a sub-horizontal fabric marked by the alignment of elongate lithic and pumice clasts (e.g. Fig. 5d) and a strong fabric of horizontally aligned biotite crystals (Fig. 4d). In some localities, lithic clasts display an imbrication that provides information on the pyroclastic flow direction at that locality.

Outcropping contacts between ignimbrite outcrops and the underlying basement or palaeosurface provide key insights into the flow conditions of the parent pyroclastic flows. Contacts are rarely exposed in proximal and medial localities but are often seen in distal localities (localities 3, 4, 6 and 11; Figs. 2 and 3; Table 1). In particular, based on preserved deposit geometries, the pyroclastic flow system responsible for producing the CGI flowed over a palaeotopography of valleys and ridges at some distal locations. In these settings, there are locations where the CGI fills palaeovalleys, but additionally, it also occurs on the palaeotopographic ridges bounding these valleys. At such locations, it might be expected that typical valley pond to ignimbrite veneer facies transitions would be found (e.g. Walker et al. 1980, 1981). A number of these distal localities are described here to provide an understanding of the nature of the pyroclastic flows and their interaction with palaeotopography. Table 1 provides a summary of key features at each of these localities.

Locality 1: Diamante

The Diamante (Fig. 3, "Introduction" section; see Fig. 2 and Table 1 for locality details) exposure represents a medial exposure of the CGI and is located along the margin of a broad south-southwest to north-northeast oriented palaeovalley, 7 km north of the topographic caldera rim and ~19 km north of the inferred caldera structural margins. The basal contact with Neoproterozoic Pachamama Schist is

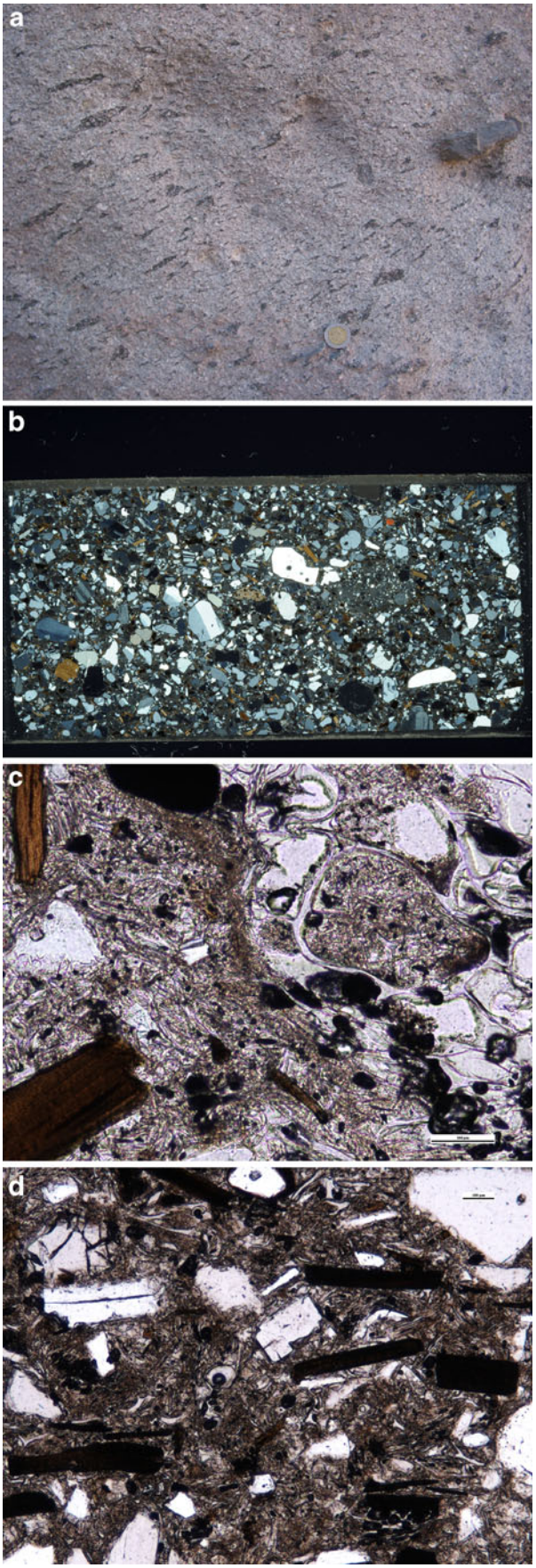

Fig. 4 Textures and components of the Cerro Galán ignimbrite. (**a**) ▶ Strong eutaxitic texture defined by flattened pumice fragments ('fiamme') and aligned lithic clasts. Note coin for scale, lower central. **b** Whole thin section view of the crystal-rich nature, with abundant volcanic quartz, plagioclase and lesser biotite and sanidine. Field of view 2×5 cm, crossed nicols. **c** Photomicrograph showing pumice and bubble wall shards in the vitric matrix of the ignimbrite. Note 100 μm scale bar *lower right*. **d** Photomicrograph showing strong biotite alignment in non-welded ignimbrite. Note 100 μm scale bar *top right*

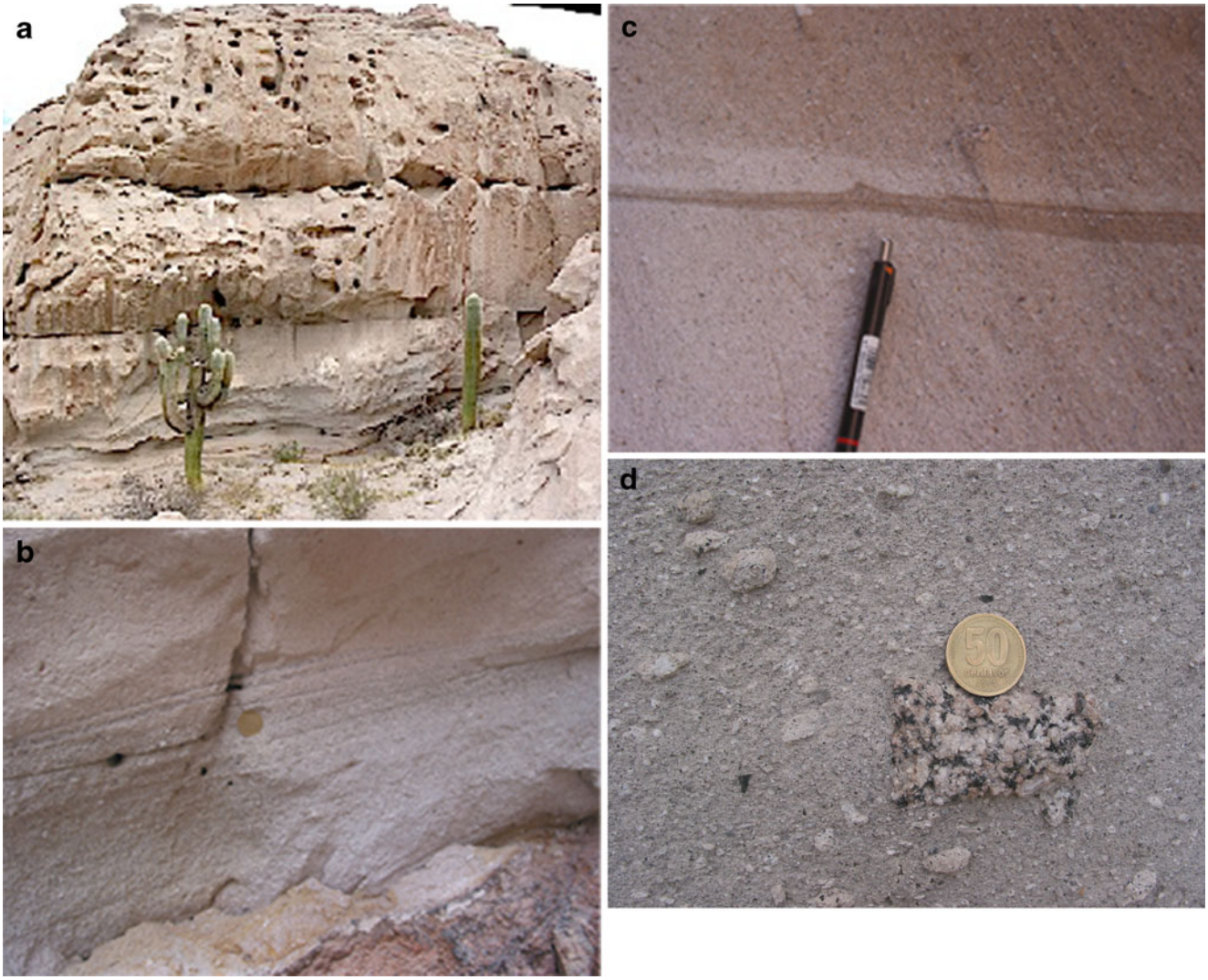

Fig. 5 Outcrop of Cerro Galán Ignimbrite at Tacuil (locality 3). **a** Outcrop of lowest four depositional units. **b** Diffusely stratified surge deposit with a flame structure at the base at its contact with the underlying palaeosoil. This is a lateral surge deposit of ignimbrite depositional unit 2 and is overlain by ignimbrite unit 3. **c** Thin, crystal-rich, fines depleted surge layer, with a small flame structure at the top, at the contact between ignimbrite depositional units 3 and 4. **d** Texture of ignimbrite unit 6, with sub-horizontal alignment of crudely rounded, elongate pumice clasts, in a crystal-rich (quartz, sanidine, plagioclase, biotite) matrix and a coarse basement granite clast

not exposed, but the section is within a few metres of outcrop of the basement defining the palaeovalley margin. The outcrop consists of one depositional unit that is >42 m thick. Lithic clasts are predominantly locally derived or accidental lithic clasts, which include dominantly metamorphic to igneous clasts derived from the Pachamama Formation with subordinate plagioclase phyric dacite. Lithic content is relatively high compared to other CGI outcrops. Lithic clasts are up to 13 cm in maximum dimension with an average of ~2 cm. The deposit lacks a clear sub-horizontal fabric at the base, but a sub-horizontal fabric defined by aligned lithic and pumice clasts is common throughout the rest of the section. AMS flow directions at the base of the section indicate north-eastward flow, but at the top indicate flow to the north-northeast (Lesti 2010; Fig. 2; Table 2).

Locality 2: Aguas Calientes

The Aguas Calientes River (Fig. 3, "Geological setting" section; see Fig. 2 and Table 1 for locality details) is incised into a palaeovalley axis north of the Galán caldera. This medial locality is located ~12 km north of the topographic rim and 25 km north of the inferred caldera collapse fault. Though the basal contact is not exposed, the thickness is relatively well constrained by an underlying fluvial conglomerate unit a few metres below section. No depositional unit breaks are visible in the entire 58-m-thick section (Fig. 3). The basal few metres show reverse coarse tail grading of both lithic and pumice clasts. The whole deposit is generally massive and is more pumice rich and lithic poor than the Diamante outcrop, including up to 20%

Table 2 Summary of location and results for AMS palaeoflow directions at specific sections where sampling for AMS studies were undertaken

	Locality	Latitude *X*	Longitude *Y*	Sample ID[a]	K_m (10^{-06} SI)[b]	Inferred flow direction[c]	E_{1-2}[d]
1	Diamante	0713885	7153998	M56	4,052	N51°	14
1	Diamante	0714174	7153988	M55	6,838	N354°	14
1	Diamante	0714174	7153988	M57	7,592	N27°	24
2	Aguas Calientes	0714430	7159589	M02	7,112	N14°	20
3	Tacuil	0753733	7169457	M41	3,469	N13°	56
3	Tacuil	0753733	7169457	M42	4,858	N2°	15
4	N of Hualfin	0757643	7155690	M45	3,469	N125º	32
5	Laguna Media	0693161	7093229	M99	6,943	N230°	11
10	Curuto	0666263	7133247	M79	13,738	N313°	6
10	Curuto	0666263	7133247	M80	14,839	N270°	18
10	Curuto	0666238	7133099	M81	11,014	N138°	18
11	Ojo de Curuto	0666245	7133011	M83	13,862	N220°	22
11	Ojo de Curuto	0666245	7133011	M84	12,825	N268°	11
12	Puntas Negras	0674201	7138927	M87	3,900	N294°	14
12	Puntas Negras	0674201	7138927	M88	4,126	N267	22
13	Punilla	0667350	7137156	M36	2,222	N242°	34
15	Beltran run-up	0676278	7158826	M66	4,001	N32°	47

See Lesti (2010) for detailed data sets and results, which are currently being prepared for publication

[a] Refer to Fig. 3 for stratigraphic locations of each sample

[b] K_m is the magnetic susceptibility (see Lesti 2010)

[c] Inferred flow direction from Lesti (2010)

[d] E_{1-2}=the semi-angle of the 95% confidence ellipse around the K_{max} axis in the foliation plane

pumice, with a maximum lithic clast size of 9 cm and average size <1 cm. The AMS determined flow direction was towards 014° (Lesti 2010; Fig. 2; Table 2).

Locality 3: Tacuil

The Tacuil (Figs. 3 and 5; see Fig. 2 and Table 1 for locality details) exposure lies almost 43 km northeast of the caldera rim and 50–57 km from structural margin assuming a simple, direct flow path, although this could have been greater and less direct given the irregular palaeotopography of the area. The exposed base of the ignimbrite succession at Tacuil is a palaeovalley margin contact with palaeosoil that is developed on metamorphosed granite, in a palaeovalley that slopes from north to south. The ignimbrite sequence is about ~60 m thick, consisting of six depositional units (Fig. 3—column 3). The four lowest ignimbrite depositional units are each underlain by a thin 3–20 cm thick, massive to planar to low angle cross-stratified deposit (Figs. 3 and 5a–c), each of which is dominated by coarse ash to fine lapilli, with only a minor fine-ash component. They are markedly fines depleted relative to the matrix of the ignimbrite depositional units. The upper contacts of these deposits, which are contacts with the next ignimbrite depositional unit, are commonly sharp and occasionally marked by flame structures (Fig. 5b, c).

In contrast, the upper two ignimbrite unit boundaries are marked by sharp planar partings and changes in pumice and lithic clast concentrations. The six ignimbrite depositional units represent the highest number of depositional units recorded anywhere in the CGI. The basal units are up to 5 m thick and become progressively thicker upwards to at least 20 m thick. The lowest two depositional units thin and wedge against the palaeovalley wall, where basal co-ignimbrite surge deposits irregularly mantle basement topography. In contrast, the tops of units are sub-horizontal, indicating valley ponding. The contact with palaeodepositional surface is irregular, and small lithic clasts of granite basement up to 2–3 cm in length are found within the ignimbrite sequence close to the contact. Clasts of granite up to 8 cm long also occur, especially in the higher depositional units (Fig. 5d).

The proportion of pumice clasts increases upwards in the sequence, up to 20 modal% pumice clasts at mid-section with clasts being up to 8 cm in maximum dimension. The size and proportion of matrix crystals generally increase up-stratigraphy. A strong sub-horizontal fabric of flat lithic and elongate pumice clasts and biotite crystals is well developed within the whole ignimbrite succession. The AMS palaeoflow directions at the base of the succession are parallel to the valley axis, but the direction higher in the sequence ‘meanders’ to the north-northeast (Lesti 2010; Fig. 2; Table 2).

Locality 4: Hualfin

The Hualfin (Figs. 3 and 6; see Figs. 1 and 2 and Table 1 for locality details) exposure lies 40 km east-northeast of the caldera rim (46–52 km from structural margin assuming a simple direct flow path), within the axis of a north-northwest to south-southeast trending palaeovalley, although the topography is now largely inverted, with the ignimbrite outcropping as a mesa (Fig. 6a). The preserved ignimbrite succession is about 55 m thick and consists of three depositional units (Fig. 3—column 4). A thin (1.5-cm) ash layer underlies the ignimbrite outcrop and overlies a granite-cobble bearing palaeosoil. The basal ignimbrite unit is up to a metre thick but wedges out laterally against basement topography (Fig. 6b) and is underlain by a coarse crystal-rich, planar to cross-stratified deposit that overlies the underlying basement topography and the ash layer. The basal thin ignimbrite unit is overlain by a 40-cm-thick planar to low angle cross-stratified deposit, which underlies the second massive ignimbrite unit (Fig. 6b) that is up to 35 m thick.

Fig. 6 **a** Cerro Galán Ignimbrite outcrop at Hualfin (locality 4), forming a mesa. The CGI sits in the axis of a palaeovalley, but modern erosion has produced inverted topography. The ignimbrite is 55 m thick for scale. **b** Basal two ignimbrite units at Hualfin in contact with a palaeosoil on basement. Note the thinning, wedging form of the lowest, thin ignimbrite because it is ponded in the axis of the palaeovalley and wedges out against the palaeoslope. Diffuse stratification in the lower and left part of ignimbrite unit 1 and sub-horizontal stratification at the base of ignimbrite unit 2 represent ground surge deposits to both ignimbrites. The lowest ignimbrite unit is 1 m thick at the lower right side of the photo for scale

Higher up the palaeovalley basement slope, a second planar to low angle cross-stratified deposit rests directly on basement, with the lower ignimbrite unit being absent. The third and uppermost massive ignimbrite unit is >20 m thick and is also underlain by a very thin 10-cm thick planar to low angle cross-stratified deposit. The middle ignimbrite and planar to low angle cross-stratified units contain the only accretionary lapilli found in the CGI, suggesting local effects, probably due to the interaction of the flow system with a local surface body of water. The whole sequence is relatively lithic and pumice clast poor, lacking the large pumice clast population found at Tacuil. There is also a weak sub-horizontal fabric of aligned pumice and lithic fragments. The AMS palaeoflow direction is to the east-southeast, at an angle of about 30° to the inferred palaeovalley axis (Lesti 2010; Fig. 2; Table 2).

Locality 5: Laguna Media

The Laguna Media (Fig. 3; see Figs. 1 and 2 and Table 1 for locality details) outcrop is located 18 km south of the topographic caldera margin and ~27 km south of the inferred collapse margin. It is the southern-most continuous section that we investigated, running up a northward sloping basement ridge slope. The base of the outcrop is not exposed, but the current outcrop is over 20 m thick (Fig. 3—column 5). A single depositional unit is massive and pumice and lithic poor, containing 5% pumice and <1% lithics. Imbricated lithics at ~10 m from the bottom of the outcrop indicate southward flow. At the top of the exposure, there is a concentration of large lithic blocks (average 40 cm diameter) and pumice clasts (15 modal%; average 1 cm diameter) that are aligned sub-horizontally. Within 5 m of the basement outcrop, the ignimbrite is noticeably more pumice rich (15–20%). The AMS palaeo-flow direction was to the southwest (Lesti 2010; Fig. 2; Table 2).

Locality 6: El Toro

The El Toro (Fig. 3; see Figs. 1 and 2 and Table 1 for locality details) outcrop is located at the distal-most extent of the CGI to the southwest of the caldera (~33 km from the topographic rime and 36 km from the inferred collapse

fault). The basal contact of the CGI is sharp, planar and inclined to the north, and the unit is 25 m thick (Fig. 3—column 6), overlying a cobble conglomerate and a basement garnet mica schist. The basal 1 m of the unit contains two lithic-rich lenses (Fig. 3—column 6), which thicken and thin laterally, and with lithologies mirroring those in basement exposure below. These concentration zones contain up to 30% lithics, with an average lithic clast size >2 cm, and elongate lithic clasts are aligned sub-horizontally. Above these concentration zones, the unit is massive and pumice and lithic poor (3% pumice, 2–3% lithics).

Locality 7: Antofagasta de la Sierra

Near the town of Antofagasta de la Sierra (Fig. 3; see Figs. 1 and 2 and Table 1 for locality details), 32 km west of the topographic caldera margin (36–38 km west of the inferred collapse fault), lies a well-exposed section of CGI that is ~14 m thick. This section contains a basal lithic concentration zone on the stoss side of an underlying N–S oriented palaeoridge consisting of fluvial conglomerate. This lithic concentration zone includes up to 65% lithics of plagioclase–phyric dacite, older ignimbrite and fine mica schist clasts in a sparse ignimbrite matrix. The clasts are identical in type and morphology to those in the nearby conglomerate. The lithic concentration zone thins at the apex of the underlying basement ridge. The deposit is massive and pumice and lithic poor above this basal lithic concentration zone with only 5% pumice and 1% lithics.

Locality 8: northwest Antofagasta de la Sierra

About 2 km northwest of the town of Antofagasta de la Sierra (Figs. 3 and 7; see Figs. 1 and 2 and Table 1 for locality details) lies a ~40-m-thick, massive pumice and lithic-poor exposure of the ignimbrite at the distal-most extent of the western CGI outflow sheet (34 km west of the topographic margin and 38–40 km west of the inferred collapse fault). The exposure lies within a few metres of a palaeoridge slope to the west, consisting of black metasedimentary pelitic schist (Fig. 7a). The CGI is generally pumice and lithic poor (2–5% pumice, 1% lithics). However, variations in ignimbrite componentry correspond with distance from the schistose basement ridge to the west. The predominance of sub-horizontally aligned lithic clasts increases towards the basement contact (up to 3% lithics). Furthermore, several discontinuous, sub-horizontal lithic clast lenses and trails of platy schistose clasts lie within tens of metres of the basement contact and give the impression of representing depositional sub-unit boundaries (Fig. 7b).

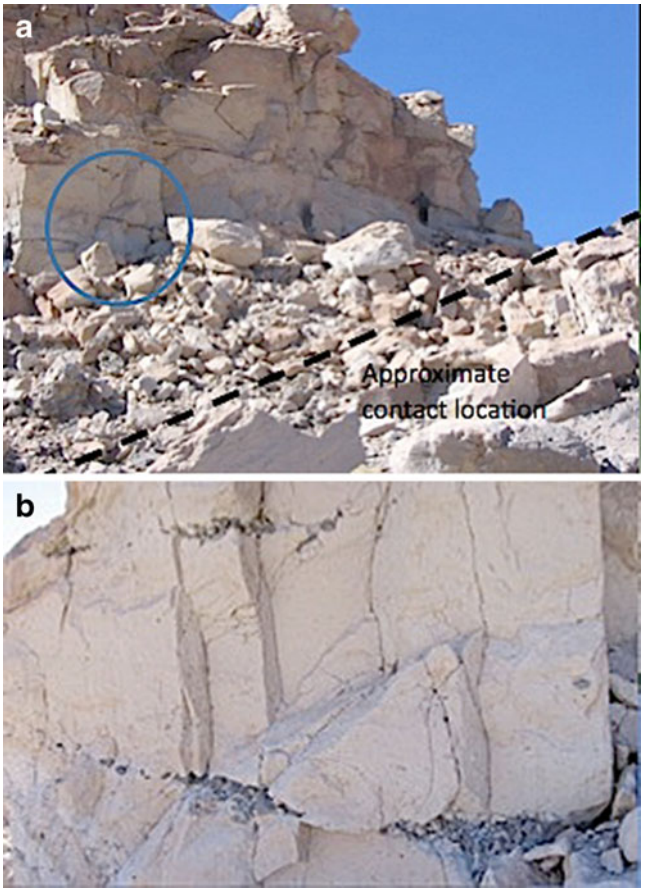

Fig. 7 **a** Outcrop of CGI 2 km NW of Antofagasta de la Sierra (locality 8), showing the location of the contact with metasedimentary basement (*dashed line*) and in the *circle part* of the outcrop shown in **b**. Note the sub-horizontal partings, which coincide with lithic clast trains. **b** Trains of metasedimentary lithic clasts, identical to the nearby exposed metasedimentary basement

Locality 9: Las Pitas Medial

The medial Rio Las Pitas (Fig. 3; see Figs. 1 and 2 and Table 1 for locality details) exposure is 19 m thick (Fig. 3—column 9) and is located 25 km west of the caldera topographic margin (~30 km west of the inferred collapse fault). It lies within a W–E-oriented broad palaeovalley and contains two distinct depositional units that sharply overlie a red, fluvial pebble conglomerate. The basal metre of the lower ignimbrite unit is reversely graded in pumice, lithics and matrix crystals, defining a 2a textural layer. Above this level, alignment of pumice clasts and vertical variations in pumice size and concentration define a diffuse but pervasive fabric and sometimes diffuse layering. Discontinuous horizontal lenses of large pumice clasts are present in the lower portion, whereas within 1 m of the top of the unit, pumice clasts are imbricated, indicating flow to the west. A pumice concentration zone is present immediately below the erosive contact with the unit above. The upper unit is defined by a basal cross-stratified layer and

overlying thin pumice concentration zone followed by a pumice-poor, reversely graded base to a pumice and lithic-poor ignimbrite (<5% pumice, average 5 mm diameter; 1% lithics, average 3 mm diameter), with a weak horizontal fabric.

Locality 10: Curuto

The Curuto (Figs. 3 and 8; see Fig. 2 and Table 1 for locality details) section lies 25 km west of the topographic caldera margin (30 km west of the inferred collapse fault). The ignimbrite is at least 25 m thick and is generally massive (Fig. 3—column 10). This outcrop is found along a basement palaeovalley contact (Fig. 8a) and shows variation in textures with distance from the palaeovalley margin. Closer to the valley axis, the basal 50 cm is pumice poor, with slight reverse grading upwards. Closer to the palaeovalley margin, a laterally discontinuous, crystal-rich, massive to diffusely stratified layer up to 8 cm thick and pinching and swelling in geometry is present at the basal contact with a local metasedimentary basement topographic high (Fig. 8b). In places, this thin basal deposit is injected into fractures in the underlying schistose basement, though the degree of interaction is variable. Immediately above the contact, pumice and metasedimentary lithic clasts are aligned sub-horizontally and show slight normal coarse tail grading; pumice concentration is low. Closer to the main palaeovalley margin, pumice clasts become more aligned (sub-horizontally) and trails of metasedimentary lithic clasts increase. Some of these trails form lenses of lithic clasts, which taper upslope (towards a basement contact). Some lithic clasts are imbricated, indicating flow to the southeast (i.e. apparently upstream and up local palaeoslope). Lithic clasts in these lenses are orientated sub-horizontally to imbricated and are tightly packed, sometimes arranged in jigsaw fit relationships, separated by thin fingers of ignimbrite matrix (Fig. 8c). Lenses of lithic clasts in one place have an en echelon arrangement, with the orientation of the enveloping surface inclined to the northeast. AMS flow directions indicate flow to the west near the base of the section, parallel to the palaeovalley axis, changing to the southeast higher up in the stratigraphy, within metres of the lateral, sloping palaeovalley wall basement contact, indicating flow away from the palaeovalley axis (Lesti 2010; Fig. 2; Table 2).

Locality 11: Ojo de Curuto

At Ojo de Curuto (Figs. 3 and 9; see Figs. 1 and 2 and Table 1 for locality details), 24 km west of the topographic margin (28 km west of the inferred collapse fault), the CGI again fills a palaeovalley and is at least 40 m thick (Fig. 3—column 11). The CGI overlies a dacite clast-rich matrix-

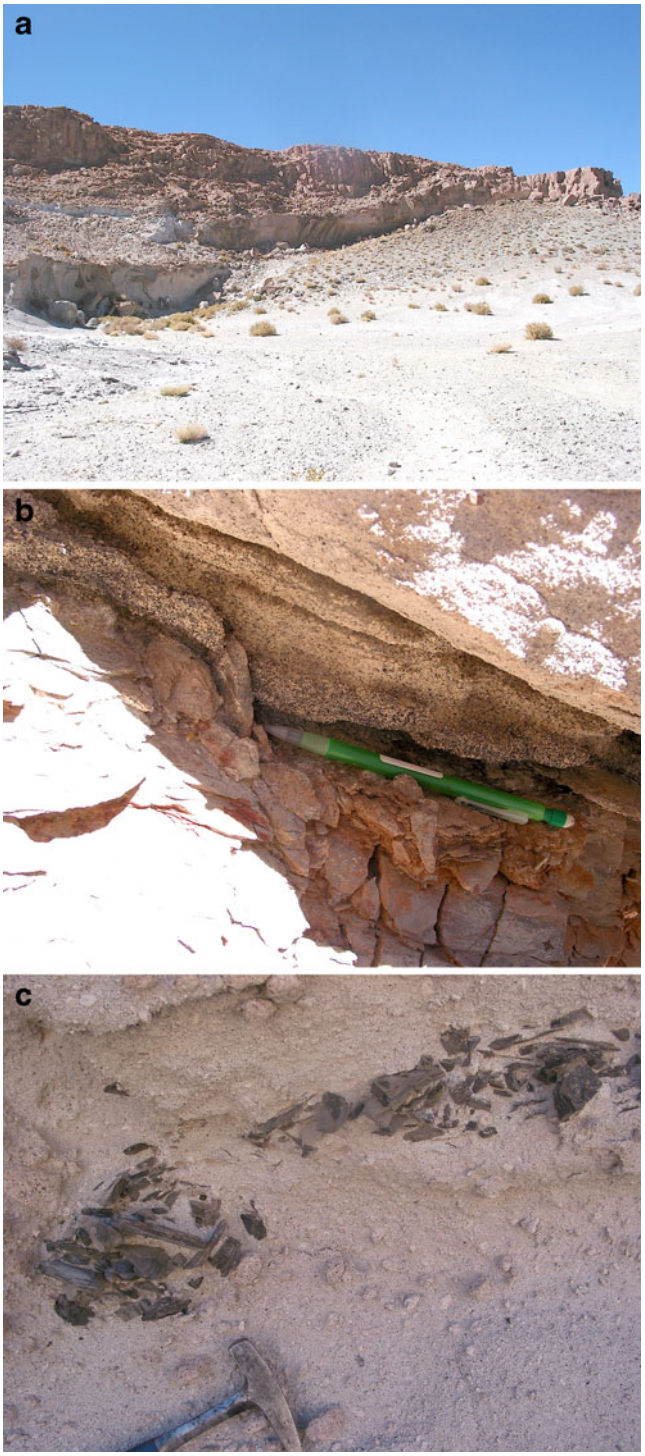

Fig. 8 Outcrop of CGI at Curuto (locality 10). **a** Overview of transition from thick valley pond (*left*) to palaeovalley slope setting (*right*). **b** Basal contact of ignimbrite against metasedimentary basement slope, showing a very crystal-rich, fines depleted, diffusely stratified ground surge, overlain by the base of the more fine-ash matrix rich ignimbrite. **c** Two en echelon lenses of platy, metasedimentary clasts, with almost jigsaw fit arrangement of some clasts, located within metres of outcropping metasedimentary pelites of identical lithology as the clast lenses

Fig. 9 Spectacular outcrop of the Cerro Galán Ignimbrite at Ojo de Curuto (locality 11). **a** Overview of transition from palaeovalley axis (*right*), where the CGI overlies basaltic andesite (*dark outcrop*) to palaeovalley slope (*centre*), where the CGI overlies dacitic debris flow deposits, to palaeoridge top deposits (*left*), which have the same massive aspect of the valley pond facies. Note the spectacular columnar jointing in vapour phase altered to weakly welded ignimbrite. **b** Non-erosional contact between the fine, coarse tail reverse graded base of the CGI and underlying debris flow deposits on the palaeovalley slope. Note the apparent red thermal oxidation of the top of the debris flow deposit

supported breccia, interpreted as a debris flow deposit, and the autobrecciated top of a basaltic andesite lava. The contact with the underlying debris flow deposit is abrupt and planar (Fig. 9). In contrast, where the flow is in contact with underlying autobreccia deposits, some lithic lenses and large lithic blocks of the basaltic andesite breccia have been incorporated into the basal part of the ignimbrite. The basal 1.5 m of the CGI is pumice poor and slightly reversely graded upwards (textural layer 2a). Throughout the outcrop, the CGI is generally massive and pumice and lithic poor (~7% pumice, 2–4% lithics). Elongate pumice and lithic clasts are commonly aligned sub-horizontally. Imbricated pumice and lithic clasts near the ignimbrite base indicate flow to the west. AMS results indicate flow to the west-southwest (Lesti 2010; Fig. 2; Table 2). High in the outcrop, the CGI overlaps onto a palaeovalley ridge and buries it. There too it is massive and lacks stratification. The total ignimbrite thickness of over 40 m, from palaeovalley floor to ridge top deposit, is made up of one depositional unit.

Locality 12: Puntas Negras

At Puntas Negras (Fig. 3; see Figs. 1 and 2 and Table 1 for locality details), 18 km west of the topographic margin (23 km west of the inferred collapse fault), a >35-m-thick section of CGI overlies the older Real Grande ignimbrite (Fig. 3—column 12). This outcrop lies in a palaeovalley margin setting, directly north of an east–west-oriented basement ridge, including Miocene age Cerro Bola, an andesite–dacite dome (Hongn and Seggiaro 2001). Although the basal contact was not observed, three distinct depositional units (Fig. 3—column 12), from bottom to top, are respectively ~8, 4 and >23 m thick. The base of the exposed section is pumice and lithic poor, with coarse tail reverse grading of pumice into an upper pumice concentration zone at the top of the lowermost unit. The overlying units are characterised by basal planar to low angle cross-stratified layers, overlain by pumice and lithic poor (7% pumice, 2% lithics), weakly stratified (defined by aligned elongate pumice clasts) deposits with occasional higher pumice concentration horizons (up to 15% pumice). AMS fabric defines a west-northwest oriented flow direction, parallel to the valley margin (Lesti 2010; Fig. 2; Table 2).

Locality 13: Punilla

The Rio Punilla (Fig. 3; see Figs. 1 and 2 and Table 1 for locality details) outcrop is located 25 km west of the caldera (30 km west of the inferred collapse fault) near the axis of a north-northeast to south-southwest oriented palaeovalley. It consists of a single depositional unit at least 30 m thick (Fig. 3—column 13) and has a pumice-poor, fines-rich base (average pumice size 3 mm), apparently representing a textural 2a layer, although the basal contact is not exposed. The overlying dominant portion of the CGI is pumice and lithic poor (5–10% pumice, <3% lithics). At a nearby lateral rise in underlying basement (dominantly basaltic andesite), a lithic-rich concentration horizon overlies basement rocks and includes clasts of basaltic andesite, plagioclase–phyric dacite and fine mica schist. Basement outcrops towards the caldera include basaltic–andesite lava flows, Miocene dacite–andesite domes and Ordovician metavolcanics (Hongn and Seggiaro 2001). AMS fabric defines a flow direction to the west-southwest (Lesti 2010; Fig. 2; Table 2).

Locality 14: Los Nacimientos

The Los Nacimientos (Fig. 3; see Figs. 1 and 2 and Table 1 for locality details) section is the distal-most CGI exposure to the west of the caldera, located approximately 30 km west of the topographic rim (35 km west of the inferred collapse fault). The basal contact of the section with underlying fluvial conglomerates and possible debris flow deposits was not observed. The CGI exposure is over 35 m thick and consists of one depositional unit only (Fig. 3—column 14). The percentage of lithics (predominantly plagioclase–phyric dacite, subordinate basaltic andesite and Ordovician meta-volcanic, derived from local basement outcrops to the east, cf. basement near Rio Punilla) is higher than at many other sections (up to 15% lithics) and shows normal coarse tail grading of lithic clasts, but pumice concentration is low (<7% pumice). Lithics and matrix biotite crystals are aligned sub-horizontally.

Locality 15: Cerro Beltran 'run-up'

The Cerro Beltran 'run-up' (Fig. 3; see Figs. 1 and 2 and Table 1 for locality details) section lies 26 km northwest of the topographic caldera rim (31 km northwest of the inferred collapse fault). The outcrop is 7 m thick, overlying the eastward dipping flank of the Miocene Cerro Beltran andesite–dacite dome (Fig. 3—column 15). The deposit is lithic poor (<2% lithics; predominantly basaltic andesite and plagioclase–phyric dacite) with intermediate pumice concentrations (5–10% pumice). AMS fabric defines a flow direction to the northeast (Lesti 2010; Fig. 2; Table 2).

Locality 16: Fulgurite yardangs

The Fulgurite yardangs (Fig. 3; see Figs. 1 and 2 and Table 1 for locality details) section lies 50 km north of the topographic caldera rim (64 km north of the inferred collapse fault). The outcrop is 20 m thick, with the true base of the outcrop not observed (Fig. 3—column 16). The deposit is lithic poor (<2%; predominantly plagioclase–phyric dacite and fine mica schist) with intermediate pumice concentrations (5–10% pumice). Between ~5 and 10 m from the base of the deposit, elongate biotite crystals in the ignimbrite matrix are aligned sub-horizontally.

Discussion of characteristics and their significance for understanding the flow behaviour of the Cerro Galán pyroclastic flow system

Depositional units

The CGI varies from a single, massive depositional unit >40 m thick almost everywhere (e.g. localities 1, 2 and 11), to multiple, massive depositional units in some distal localities (localities 3, 4 and 12). However, at no locality do we find any field stratigraphic and contact relationships that indicate significant time breaks between depositional units. These homogenous characteristics indicate a depositional system fed at constant rates that resulted in constant deposit characteristics (e.g. Branney and Kokelaar 2002). The almost exclusive existence of only one massive depositional unit up to 60 m thick (localities 1 and 2) and the presence of multiple depositional units in more distal settings cannot be ascribed to several discrete flow units being generated at the vent from separate discrete eruptions, or from unsteady flow conditions at source. Multiple depositional units occur where palaeotopography appears to have been most pronounced (localities 3, 4 and 12), indicating the onset of unsteady flow conditions in distal settings resulted from interaction between the pyroclastic flow and the palaeotopography during a single, ongoing flow event. Processes that can account for the development of topography-induced unsteadiness in the flow include its reflection and deflection along valley margins, acceleration and/or deceleration along changing sections of valleys and ridges and at breaks in slope (e.g. Fisher 1990; Fisher et al. 1993; Giordano 1998; Woods et al. 1998).

Where multiple depositional units occur (e.g. localities 3 and 4), they become thicker upwards. We interpret this to indicate that the initial part of the flow system was able to interact with topography, leading to unsteady flow and the break-up of the flow into multiple lobes (cf. Freundt and Schmincke 1986). The deposits from this early part of the flow system would have smoothed much of the pre-existing bed roughness, leading to more steady flow conditions and deposition of progressively thicker, upper massive units of the deposit. In addition, or alternatively, mass flux and particle concentration may have increased, leading to increased sedimentation rates, thus suppressing turbulence and flow unsteadiness.

Depositional unit boundaries

Depositional unit/pulse boundaries vary from being represented by planar to low angle cross-stratified deposits, to strongly defined planar partings, to variations in pumice and/or lithic clast abundance and in some cases by trails of lithic clasts. The planar to low angle cross-stratified deposits are interpreted to be from ash-cloud surges (i.e. more dilute parts) of the pyroclastic flow system (Fisher 1979). They are not fluvial sediments because their componentry is identical to the ignimbrite units above and below, they have a texturally immature character and there is no evidence of time breaks at their bases. Where lithic clast trails occur, the lithic clasts are identical to the local bedrock and are therefore locally derived accidental lithic

clast populations. The lithic clast trails only occur close to the contact with the palaeoslope bedrock outcrops. They often disappear within 20–50 m of the basement contact, causing the apparent multiple depositional units close to the basement contact to merge into a single visible depositional unit. This indicates that the accidental lithic clasts have not been transported very far from their original source (cf. Buesch 1992).

The surge deposits between ignimbrite depositional units are generally only centimetres thick (e.g. Fig. 5c) and in some cases pinch and swell (locality 4). In some cases, this represents original surge dune morphology, indicating no erosion by the base of the succeeding pyroclastic flow. In other cases, some truncation at the base of the overlying ignimbrite unit is visible, but the amount of erosion seems minor (cf. Fisher 1979). The surge deposits are markedly more fine-ash depleted than the underlying and overlying ignimbrite depositional units, indicating more expanded, probably more turbulent flow conditions, at the depositional boundary layer than those developed by higher concentration zones in the body of the pyroclastic flow (Cas and Wright 1987).

If, as seems to be the case based on field evidence, we are dealing with one continuous flow event sustained over time, this suggests that lower particle concentration turbulent surge cells can form very quickly in a flow system, even in distal localities (Fisher 1979). Furthermore, the variation in the number of surge deposits and our inability to correlate them and associated ignimbrite depositional units between localities indicate that generation of the low particle concentration turbulent surge cells is also a local effect, again due to the effects of local topography on the pyroclastic flow system.

Relationships between the CGI and palaeotopography

The Cerro Galán Ignimbrite was dispersed and is preserved radially all around the caldera. The current outcrop area of the CGI is about 2,400 km^2, but estimates of the effects of post-emplacement erosion indicate that the original extent has been reduced by at least 50% (Folkes et al. 2011a). Although outcrops extend up to 80 km from the structural margin of the caldera, the original maximum flow distance reached would have been greater, except in places where topography constrained flow mobility. To estimate the aspect ratio (AR) of the CGI, we have taken an average radial runout distance of 50 km as an absolute minimum and an average deposit thickness of 45 m (see Folkes et al. 2011a). Using AR=H/L where H=average thickness and L =diameter of a circle of the same (original) surface area as the ignimbrite (therefore in this case L=100 km), the AR of the CGI originally would have been 4.5×10^{-4}.

The surface of the CGI forms a sloping plateau (Fig. 2b), sloping radially away from the caldera. Selected radial profiles (A–B, E–F; Fig. 2a) suggest that the mean slope of this plateau is 8–9°. Only at some distal localities did the ignimbrite climb topography, reaching up to 250 m above the local base of slope.

Depositional unit boundaries are generally sub-horizontal, and on-lap the palaeotopographic slopes with contacts parallel to the plateau surface rather than mantling the topography. Where thin depositional units impinge against more steeply sloping, local basement slopes they wedge out against the slope. In addition, where the CGI has in-filled palaeotopographic lows/valleys and has surmounted and been deposited onto inter-fluve palaeoridges, there is no typical stratified ignimbrite veneer facies, as has been documented for small-to-moderate volume ignimbrites (e.g. Walker et al. 1981; Wilson 1985; Freundt and Schmincke 1986; Nakada and Fujii 1993; Giordano et al. 2002; Pittari et al. 2006). This indicates that the mass flux of material in the flow and depositional system and the particle concentration was consistently too high to produce stratified to cross-stratified and finer-grained ignimbrite veneer facies typical of small-to-moderate volume ignimbrite deposits on topographic highs. It also suggests that the upper parts of the flow system were not as dynamic and turbulent as in smaller volume, more dynamic counterparts. Although it could be argued that veneer facies formed and were eroded, the lack of any veneer deposits in the Cerro Galán Ignimbrite suggests they did not form and that this is related to the flow behaviour of this type of large volume ignimbrite. This is furthermore supported by the preservation of the multiple thin surge deposits in palaeovalley settings, but not veneer deposits on ridges.

AMS fabric and relationship between palaeoflow directions and palaeotopography

The CGI consistently developed a sub-horizontal AMS depositional fabric at all locations where AMS fabric has been analysed. This is consistent with the sub-horizontal pumice, lithic clast and even biotite crystal fabric commonly found in the CGI throughout its extent and at all stratigraphic levels.

In localities where original palaeotopography can be reconstructed, the flow directions appear to have been along palaeovalley axes, particularly near the base of the deposit where the flow was most confined by topography. At localities where more than one sample has been collected and analysed, there are variations in flow direction up-sequence (e.g. localities 1, 3, 10, 11 and 12 in Fig. 2), generally at slight to moderate angles of up to 40° to the palaeovalley axis trend. There is only one locality at Curuto where the AMS flow direction is almost at right angles to the palaeovalley axis, indicating the flow was upslope, up the valley walls, which is consistent with the flow

expanding sideways up the valley wall with time. At all other sample localities at Curuto, AMS flow directions are sub-horizontal and parallel to palaeovalley axes. Elsewhere, the flow direction is more variable where palaeotopography was gentle or flat, suggesting meandering behaviour in unconfined topography.

Lithic clast content and distribution

As previously mentioned, lithic clasts make up a minor proportion of the CGI (<3% by volume). Although some porphyritic dacite clasts could be vent-derived, most clasts appear to be accidental lithic clasts, derived from nearby granite, slate/schist or older dacite basement outcrops. Lithic clasts rarely reach greater than 20 cm in size and are most commonly only a few centimetres to less than a centimetre in size. Lithic clasts are evenly distributed throughout the ignimbrite and commonly have a sub-horizontal orientation. In some places, a low angle imbrication is observed. Occasional lithic concentration horizons occur, but only locally (e.g. localities 6 and 7) and are not a regionally extensive facies of the CGI.

Furthermore, in some localities, lithic clast clusters form 'jigsaw' fit domains of clasts (localities 7 and 10). Here, clasts are separated by thin fingers of ignimbrite matrix, indicating that individual clasts were derived from a single fractured larger clast, which has been barely disaggregated during transport. It was therefore almost certainly derived from nearby basement palaeoslope and/or was transported in a relatively passive, non-turbulent manner. Where the basement slate sequence crops out (e.g. northwest of Curuto, localities 8 and 10), it is pervasively cleaved, and debris is spalling off the outcrops. It is therefore surprising how little lithic debris occurs in the ignimbrite, suggesting the pyroclastic flow applied a low lateral shear stress to the substrate.

As reported by Lesti et al. (2011), TRM analysis of lithic clasts indicates that the CGI was emplaced at high temperatures (≥600°C), and this is verified by variable degrees of welding of the ignimbrite to the north, east and south (e.g. Fig. 4a).

Pumice clast content and distribution

The content of lapilli to bomb size pumice clasts in the CGI is also commonly low (<10%), with such clasts evenly distributed through the ignimbrite. However, in some localities, higher concentrations of large pumice clasts occur at specific levels, defining pumice concentration horizons and probably depositional pulses (e.g. locality 3, Tacuil; locality 12, Puntas Negras). Pumice clasts appear to be more common close to palaeotopographic slopes than in nearby valley pond settings (e.g. locality 10, Curuto), perhaps indicating a rafting of low density pumice clasts away from the central axis of flow and towards the margins against valley walls. Elongate pumice clasts are also commonly sub-horizontally orientated (e.g. Fig. 5d).

Ignimbrite texture and granulometry

Apart from the rare surge deposits, which are markedly fines depleted and relatively well sorted, the ignimbrite is uniformly poorly sorted, massive, with low lithic and pumice clast content dispersed in an ash matrix that constitutes >80% of the ignimbrite. The ash matrix consists of about 50% coarse crystal fragments (>1 mm) and 50% fine-ash particles. A strong sub-horizontal fabric of aligned lithic and pumice clasts is common and is visible in all outcrops to varying degrees and at all stratigraphic levels in the ignimbrite. Even biotite crystals are commonly aligned sub-horizontally, a fabric that is readily visible in outcrop at all levels in the ignimbrite and even more so in thin section (e.g. Fig. 4d). In some locations, feldspars are also aligned with a sub-horizontal orientation.

Implications for flow dynamics at the time of deposition in distal settings

The massive nature of the ignimbrite indicates high depositional rates. Tractional structures, such as cross-stratification and undulating planar lamination, are limited to only a few locations where thin surge deposits separate depositional pulses/units of massive ignimbrite, without evidence of intervening palaeosoils or other evidence for time breaks. Throughout the CGI, there is a strong sub-horizontal fabric that remains so at contacts with sloping basement palaeovalley walls, indicating that palaeotopography was filled progressively, or incrementally by on-lap under relatively passive flow conditions. Thin depositional units also wedge and taper up palaeovalley walls. The horizontal on-lap fabric is defined by local thin horizontal surge beds, horizontal trails of lithic and/or pumice clasts, horizontal ignimbrite horizons that are more pumice rich than the ignimbrite above or below, aligned horizontal elongate lithic and pumice clasts and even aligned horizontal biotite flakes and sometimes feldspar crystals. These fabrics indicate that there was a constant horizontal depositional shear force throughout CGI deposition that induced horizontal alignment of pyroclasts from large fragments to ash size fragments. However, the generally low lithic content indicates limited erosional capacity of the pyroclastic flow system.

There is no evidence that any part of the flow system flowed up and over topography higher than the main part of the flow system confined within the valley, in that there are no visible fabrics or bedding that mantles or dips parallel to sloping palaeovalley walls. All indications are that at all distal settings, the flow system was confined to and filled in

the lowest point in the topography along the flow path, before filling and progressively lapping onto the palaeotopographic slopes and ridges. This is confirmed by AMS flow direction data showing that where palaeotopography existed, flow was almost always parallel to the axes of palaeovalleys. Only higher in the CGI outcrops, where palaeovalleys had already been variably in-filled and were more open, did the flow paths deviate by up to 40° (Lesti 2010). Flows were not energetic enough to expand and spread sideways and flow up the valley walls orthogonal to valley axes, except at one locality at Curuto.

Where palaeovalleys were eventually filled in, the CGI spread and was deposited on top of and buried inter-fluve ridges. The absence of typical stratified and finer ignimbrite veneer deposits anywhere on palaeotopographic ridges is also consistent with relatively passive infilling and drowning of topography by a flow system similar to that in valley pond settings, with apparently high particle concentrations and little or no evidence for substantial turbulence.

Only in a few locations does the flow system appear to have broken into discrete flow pulses that also produced surges between the flow pulses. These locations (3—Tacuil, 4—Hualfin and 12—Puntas Negras) occur where local palaeotopographic relief between valley floor and ridges was the highest, suggesting that the flow system became unsteady in highly irregular terrain and split into multiple ephemeral flow pulses that followed each other in rapid succession. Surge deposits between depositional units are thin and fines depleted, indicating higher levels of turbulence, flow expansion and hydraulic sorting than in the intercalated massive ignimbrite depositional units. The preservation of these thin surge horizons between massive ignimbrite units, without being eroded, testifies to a relatively non-energetic, non-erosional flow state in general in the pyroclastic flow system. Only at Las Pitas Medial (locality 9) is there more than one depositional unit in a situation where there is no outcropping basement ridge. Fisher (1979) proposed that in medial areas, flow systems develop multiple vortices or flow cells, each of which may undergo density segregation. This may well be true, but this tendency would be enhanced by interaction of the flow system with significant topography as is the case for the CGI. Perhaps at Las Pitas Medial there is an unseen basement ridge, or the flow system was disturbed by having to diverge around the large Cerro Merihuaca edifice to the north.

Lithic clast abundance is low (<3%), and locally derived lithic clasts are small (generally <5 cm), suggesting very low erosional capacity of the pyroclastic flow system in a landscape where the ground surface, as today, would have been littered with loose bedrock debris. The presence of local basement-derived lithic trails and jigsaw fit basement lithic clast clusters, which occur only close to contacts with basement, indicate local derivation and only limited transport distance of those lithic populations from their source. The preservation of lithic clast clusters and sub-horizontal trails of locally derived lithic clasts is consistent with limited turbulence, a horizontal shear force strong enough to move the clasts, but limited capacity to carry lithic clasts far from their source point. If the pyroclastic flows had been highly turbulent, jigsaw fit clast clusters would have been disaggregated and the individual clasts chaotically mixed throughout the ignimbrite.

Furthermore, the low abundance of vent-derived or accessory lithic clasts (dominated by a plagioclase–phyric dacite proportion) and the absence of lag breccias, lithic concentration zones and ground breccias/layers likely reflect the sparsity of erupted vent-derived lithic debris due to the eruption dynamics (Sparks et al. 1985). However, this also indicates a flow system that was largely incapable of eroding and transporting coarse (>20 cm diameter), or even abundant (<1%) lithic debris from the vent area.

In summary, the CGI pyroclastic flow system appears to have been a relatively low energy, low velocity pyroclastic flow system, with limited erosional capacity, that flowed radially, down a slope of about 8–9° away from the caldera as a high particle concentration, granular flow. Such flow conditions appear to have been relatively constant throughout the duration of the eruption. The widespread horizontal alignment fabric affecting all grain sizes and all components indicates a pervasive shear force at the scale of grains during deposition. The poor sorting, abundance of fine ash, the limited erosional capacity and horizontal depositional fabric are consistent with a high particle concentration, essentially laminar, basal, shearing granular flow with suppressed turbulence. The consistent sub-horizontal AMS fabric also supports this, as also noted by Knight et al. (1986) in their study of the giant Toba Tuff in Indonesia.

It is possible to calculate the minimum force and dynamic pressure that would have been exerted by the pyroclastic flow (Valentine 1998) and the minimum flow velocity required to move lithic clasts from a position of rest on the substrate, assuming a horizontal trajectory of movement along a valley wall, using the approach of Pittari et al. (2007; the reader is referred to that paper for the derivation of the following equations and physical parameter values). Most physical parameters are fixed in this approach, with the main variable being the bulk density inferred for the pyroclastic flow. We have argued that the flow system was a high particle concentration, shearing granular flow. Since macroscopic pumice and lithic clasts are minor components, the dynamics of the flow would have been controlled by the properties of the matrix components and the particle packing density, or proportions of solids to gas. The gas has a negligible density. For these calculations, we have taken the

matrix to consist of 50% crystals and lithic fragments with a mean density of 2,650 kg m^{-3}, 25% vesicular pumiceous fragments with a vesicularity of 60% and a DRE density of 2,650 kg m^{-3} and fine-ash glass shards without internally trapped vesicles, which therefore also have a density of 2,650 kg m^{-3}. The weighted bulk density of the solids is then 2,400 kg m^{-3}. We have chosen two end-member particle packing densities. The maximum of 60% particles to 40% gas corresponds to practical limit before total frictional interlocking would render the flow immobile. The lower concentration of ~45% particles provides close but free space between all particles. The latter is consistent with the packing density proposed by Branney and Kokelaar (2002) for dense pyroclastic flows capable of flowing into and under water. Using these proportions of solids to interstitial gas, this then gives pyroclastic flow bulk densities of ~1,440 and 1,080 kg m^{-3}, respectively, which we will use in the following calculations of dynamic pressure and flow velocity.

Essential equations are:

1. The force required to move a static boulder of granite gneiss or slate 0.2×0.2×0.2 m in dimension, resting on bedrock, is given by:

$$F_1 = u_s mg \tag{1}$$

2. The force applied to a boulder at rest by a pyroclastic flow is:

$$F_2 = 0.5\rho_{fl} v^2 C_D A \tag{2}$$

3. Dynamic pressure, or power, exerted by a pyroclastic flow is a product of the bulk flow velocity, v (metres per second), and the bulk flow density, ρ_{fl} (kilograms per cubic metre). Dynamic pressure, P_D (kilopascal) is given by:

$$P_D = 0.5\rho_{fl} v^2 \tag{3}$$

where

- The maximum lithic clast dimensions=0.2×0.2×0.2 m
- Clast volume, v=0.008 m^3
- Clast surface area impacted by the flow force, A=0.04 m^2
- Density of the two main locally derived basement clast lithologies, slate and granite gneiss, ρ_c both ~2,700 kg m^{-3}
- Clast mass, m=21.6 kg
- Coefficient of static friction, u_s=0.7
- Acceleration due to gravity, g=10 ms^{-2}
- Coefficient of aerodynamic drag, C_D=0.8
- Assumed bulk density of the pumiceous pyroclastic flow, ρ_{fl}=1,440 or 1,080 kg m^{-3}
- Pyroclastic flow velocity, v
- Dynamic pressure exerted by a pyroclastic flow, P_D

Therefore, the minimum force required to move a static boulder of granite gneiss or slate 0.2×0.2×0.2 m in dimension, resting on bedrock using Eq. 1, is 151.2 N.

However, the force applied to a boulder at rest by a pyroclastic flow using Eq. 2 is:

$$\begin{aligned} F_2 &= 0.5\rho_{fl} v^2 C_D A \\ &= 0.5 \times 1,440 \times v^2 \times 0.8 \times 0.04 \text{ OR} \\ &= 23v^2 \text{ or } 17v^2 \end{aligned} \tag{2}$$

If we equate, Eq. 1=Eq. 2

$$23v^2 = 151.2, \text{ or } 17v^2 = 151.2$$

Then the minimum flow velocity required to move the boulder is v=2.56 ms^{-1} (= 9.2 km h^{-1}) or 2.98 ms^{-1} (= 10.7 km h^{-1}), respectively. The dynamic pressure exerted by the pyroclastic flow using Eq. 3 is 4.7 kPa for both bulk flow densities.

We believe these perhaps surprisingly low values accurately reflect the low power and flow velocity of the Cerro Galán pyroclastic flow system because our field evidence indicates that locally derived basement lithic clasts were not transported far from their bedrock source point (tens to hundreds of metres only), and jigsaw clusters of basement-derived lithic clasts are still preserved.

By comparison, the calculated velocity of small volume Mt Unzen, Japan, block and ash flows in 1991 were 15–25 ms^{-1} (~70–80 km h^{-1}; Yamamoto et al. 1993). Maximum velocities for the June 25, 1997 pyroclastic flows and surges on Montserrat from the Soufriere Hills volcano were about 50 ms^{-1} (~180 km h^{-1}) generating dynamic pressures of 2–2.4 kPa (Loughlin et al. 2002). Pittari et al. (2007) estimated dynamic pressures from 5 to 38 kPa and velocities up to 87 ms^{-1} (>300 km h^{-1}) for the lithic-rich Abrigo Ignimbrite on Tenerife. The Taupo 186 AD pyroclastic flow in New Zealand is estimated to have experienced flow velocities of at least 250–300 ms^{-1} (940–1,080 km h^{-1}) in proximal areas to 150 ms^{-1} (540 km h^{-1}) in distal areas (Wilson 1985). For the Mt St Helens 1980 lateral blast flow, early velocity estimates were ~235 ms^{-1} (>800 km h^{-1}; Kieffer and Sturtevant 1988), but in a more recent estimate, Esposti Ongaro et al. (2011) calculate a velocity of 140 ms^{-1} (~500 km h^{-1}) medially and 70 ms^{-1} (250 km h^{-1}) distally. Calculations for the

dynamic pressure range from >100 kPa in proximal to distal areas to 0.5–10 kPa in distal areas (Esposti Ongaro et al. 2011).

By comparison, calculations for the March 11 2011 Japanese tsunami flow velocity on-land, based on analysis of video footage, range from 5 to 7 ms^{-1}, but generally less than 10 ms^{-1} (S. Kieffer, personal communication). However, the velocity of the flow in chutes between buildings may have been up to 10 ms^{-1}, similar to flow velocities in the rapids of the Colorado River. Using a bulk density of 1,000 kg m^{-3} and end-member velocities of 5 and 10 ms^{-1}, the dynamic pressure exerted by the wall of water would have been 12.5 or 50 kPa, essentially three to ten times more powerful than the Cerro Galán flow system seems to have been. Once the tsunami became debris laden, this would have increased significantly.

The factors that may explain the differences in flow velocities and dynamic pressure between the CGI flow system and the other examples cited above include the slope of the terrain, the column collapse height and the magnitude of lateral explosive momentum. The Mt St Helens blast flow was initiated by a tremendous lateral explosion from which it achieved its initial extremely high flow velocity and dynamic pressure, which allowed it to surmount very high and irregular topography, as well as flatten fully grown forest trees. The very dynamic Taupo pyroclastic flow is thought to have resulted from the collapse of an extremely high, ultra-plinian explosive eruption column (>50 km; Wilson and Walker 1985) that produced an extremely widespread fall deposit. It is unknown from what height in the column the material collapsed from to be fed into the pyroclastic flow. However, it is likely that the extraordinary calculated velocity and mobility can be explained from the extremely high momentum of the flow acquired from collapse from a very great height and the very high potential energy of the collapsing mass of pyroclastic debris. Flow systems such as those from Soufriere Hills, Unzen and Tenerife are thought to have originated from lower eruption columns, or summit domes. The original momentum was lower, but all three volcanic edifices have steep upper slopes, which therefore generated moderately high flow velocities and dynamic pressures, although not as high as either the Mt St Helens blast flow or the Taupo flow. By contrast, the CGI flow system is interpreted to have originated from a sustained low, fountaining eruption column and flowed down a relatively gentle, radially sloping ignimbrite shield surface of about 8–9°. It probably never had high momentum and therefore flowed at velocities and produced dynamic pressures, considerably lower than for the other examples cited. Volatile content would also play a part in determining column height as well as the density of the pyroclast components.

Comparing the CGI and flow system with other ignimbrites and their flow systems

Ignimbrites have been subdivided into high (HARIS) and low aspect ratio ignimbrite (LARIS) end-member types (Walker et al. 1980; Walker 1983; Cas and Wright 1987; Druitt 1998; Branney and Kokelaar 2002). HARIS are relatively thick compared to their lateral extent. They are thought to result from pyroclastic flows that are generally lower in energy and flow velocity and are therefore mostly confined by topography. HARIS vary in volume from small such as the Laacher See, Germany (Freundt and Schmincke 1986); Katmai, Alaska (Hildreth 1983); Mt St Helens, USA (Rowley et al. 1981) and Pinatubo, Philippines (Scott et al. 1996) to moderate such as the Bandelier Tuff, New Mexico (Smith and Bailey 1966; Self et al. 1986) and to large such as the Bishop Tuff (Wilson and Hildreth 1997) and the Oruanui Ignimbrite (Wilson 2001). Their deposits are generally valley confined and massive to diffusely stratified but may also develop finer-grained cross-stratified deposits on adjacent palaeotopographic lows, resulting from the peripheral ash-cloud parts of the pyroclastic flow system (cf. Nakada and Fujii 1993).

Hildreth (1983) proposed that the body of the 1912 Katmai pyroclastic flow was relatively slowly moving and diverted around a 25-m-high glacial moraine, before continuing to flow a further 5 km, whereas the ash-cloud surge part, deposited stratified deposits on the moraine ridges. Similarly, Freundt and Schmincke (1986) showed that small volume flows in the Laacher See volcano in Germany also preserved deposits with valley pond and ignimbrite veneer characteristics in low relief terrain. Giordano et al. (2002) demonstrated that a small volume phreatomagmatic ignimbrite from Colli Albani volcano in Italy shows the lateral transition from the valley pond facies into the veneer facies. In one of the most detailed documented accounts of the lateral facies variations in an ignimbrite, Pittari et al. (2006) showed that the lithic clast-rich Abrigo Ignimbrite on Tenerife produced lateral transitions from massive valley pond to finer-stratified 'ignimbrite veneer' deposits where the palaeorelief was as little as a few metres. Nakada and Fujii (1993) demonstrate very efficient separation of the high particle concentration valley confined body deposits of the Unzen block and ash flows, from the detached ash-cloud surge deposits which flowed up and over nearby topography.

By contrast, LARIS are relatively thin compared with their lateral extent and are small to moderate in volume. LARIS were originally thought to originate from pyroclastic flows that could flow over significant topography because of their high inferred flow velocity and have a high erosional and dense clast carrying capacity, as reflected by coarse, layer 1 co-ignimbrite breccias (e.g.

Wilson 1985; Allen and Cas 1998). Well-documented studies of LARIS include the Taupo Ignimbrite, New Zealand, (Walker et al. 1981; Wilson 1985); the Kos Ignimbrite, Greece (Allen and Cas 1998, 2001); the Campanian Ignimbrite, Italy (Fisher et al. 1993; Rosi et al. 1996); the Villa Senni Ignimbrite, Italy (Watkins et al. 2002) and the Kizilkaya ignimbrite, Turkey (Schumacher and Mues-Schumacher 1996). All are laterally extensive, of relatively uniform thickness and have distinctive lithic-rich layer 1 co-ignimbrite lithic breccia facies. They have massive poorly sorted valley pond facies and finer-stratified ignimbrite veneer facies deposited on topographic highs (Walker et al. 1980; Walker 1983).

Walker et al. (1981) and Wilson (1985) showed that the low aspect ratio 186 AD Taupo Ignimbrite preserves massive valley pond facies in deep valleys and finer-grained stratified ignimbrite veneer facies on nearby ridges that are hundreds of metres higher. The pyroclastic flow responsible for the Taupo ignimbrite is thought to have originated from the collapse of a very high eruption column and been a very high velocity flow capable of flowing over very high topography. It had enormous erosional force, as reflected by preserved blown down tree trunks, very coarse ground breccias and high lithic contents of both vent-derived and local ground surface origin.

The CGI is very large in volume, it lacks coarse co-ignimbrite breccias and it shows no evidence that its flow system was capable of significant erosion. It is a massive deposit and lacks ignimbrite veneer deposits. These features are most consistent with it originating from a slow moving HARI-type pyroclastic flow. However, it has a low aspect ratio, which is generally associated with high velocity flow.

This apparent contradiction is readily explained by the nature of the terrain over which the pyroclastic flow system flowed. As discussed above, the CGI flow system flowed radially away from the vent on a slope of about 8° to 9°. The slope appears to have been relatively smooth, especially to the west, produced by the earlier Toconquis Group ignimbrites which had buried most previous bedrock topography in proximal and medial areas. Only in distal settings was basement topography still prominent, and there it appears the CGI flow was confined by topography, progressively filling and burying it through deposition of typical massive valley pond facies. The absence of typical ignimbrite veneer facies, even where palaeotopographic ridges have been buried, also indicates a low velocity and energy flow regime, similar to that inferred for the bodies of HARIS. This suggests that the hydraulic head of the pyroclastic flow system from the caldera rim to distal localities during a sustained, low collapsing fountain style of eruption, was enough to allow the large volume, gas fluidised flow to spread itself over a large surface area. Had the topography been flatter, or more irregular and higher in proximal to medial areas the CGI is likely to have had a HARI like geometry.

Schumacher and Mues-Schumacher (1996) also proposed that the flow that produced the moderate volume (~90 km^3) low aspect ratio Kizilkaya ignimbrite, Turkey, was slow moving, with suppressed turbulence. Most of the ignimbrite was emplaced on a flat palaeoplain, where again hydraulic head from the source area could have led to wide spread dispersal and mobility in the absence of significant topographic impediments.

There have been relatively few studies that have documented the detailed facies characteristics of widespread, very large volume ignimbrites like the Cerro Galán Ignimbrite. They can be grouped into two categories, complex and simple. Complex large volume ignimbrite successions consist of successions of multiple ignimbrite and fallout deposits (e.g. Bishop Tuff, USA, Wilson and Hildreth 1997; Oruanui Ignimbrite, Wairakei Formation, New Zealand, Wilson 2001). The ignimbrites are HARI-type ignimbrites and pyroclastic flow formation can be related to the collapse or partial collapse of the eruption column that produced the contemporaneous fallout deposits. It is unclear to what degree the eruption was interrupted to generate the multiple fall and flow deposits.

Simple large volume ignimbrites consist of a single, or a couple of large volume ignimbrite depositional unit(s), perhaps preceded by a relatively small volume fall deposit, but often without a preceding fallout deposit (e.g. Lower Panizos Ignimbrite, Bolivia, Ort 1993; Toconoa Ignimbrite, Chile, Lindsay et al. 2001; Atana Ignimbrite, Lindsay et al. 2001; Sifon Ignimbrite, northern Chile, de Silva 1989; Puripicar Ignimbrite, northern Chile, de Silva 1989). The eruptions were clearly continuous and sustained. With the exception of the Toconoa Ignimbrite, which is crystal poor and rhyolitic in composition, all the other Andean ignimbrites are similar to the CGI, in being very crystal-rich (~50%), generally rhyodacitic in composition, at least partly welded, and lacking an underlying fall deposit, suggesting a common eruption style and perhaps a similar transport regime for these large volume crystal-rich ignimbrites. Ort (1993) proposed a flow mechanism involving limited fluidisation and modified grain flow for the Panizos ignimbrite flow system.

Relevance of experimental and modelling studies to understanding the flow behaviour of very large volume pyroclastic flows

Many experimental studies and numerical simulations have been undertaken in recent years on the flow behaviour of high particle concentration granular flows (e.g. Roche et al. 2005; Dufek and Bergantz 2007; Dellino et al. 2007; Druitt et al. 2007; Dufek and Manga 2008; Dufek et al. 2009;

Giordano and Dobran 1994; Girolami et al. 2008, 2010; Valentine and Wohletz 1989; Bursik and Woods 1996). The experiments all involve instantaneous lock release of small volumes of artificial beads or natural fine-ash mixtures from ignimbrite in small experimental tanks or down ramps. Not included in this list of experiments are those involving aqueous density currents. In some experiments, the released flow materials were partially fluidised prior to release, and in some cases, they were heated (e.g. Girolami et al. 2008) to ensure there were no cohesive effects between particles due to interstitial water moisture during flow events. All such experiments produced granular flows of material. These may simulate the higher particle concentration under-flows or body parts of pyroclastic flows, but they clearly do not include the nature of the ash cloud or the transition and physical relationship between the pyroclastic flow and its enclosing ash cloud. The principal results of these experiments relevant to this study are:

- Pre-fluidised masses of grains are more mobile as released flows than non fluidised flows (Roche et al. 2006; Girolami et al. 2008).
- The mobility of experimental flows increases with finer grain sizes because the fine grain sizes trap gas more so than coarse grain size aggregates and create a situation that we call here 'hindered gas escape' that reduces the coefficient of internal friction in the flow (Roche et al. 2005; Druitt et al. 2007).
- In a flow with two principal grain sizes, when the fraction of the fine grain size population is less than the volume of space between large particles at minimum contact packing density for the large particles (30–40%), the flow behaviour is dominated by frictional interaction between the large grains and the flow is less mobile than when the fine fraction exceeds 40% of the grain population (Roche et al. 2005). At >40% fines fraction, the large grains are passively rafted along by the fines fraction, and the flow mobility or run out increases (Roche et al. 2005).
- Granular experimental flows move in a laminar flow state (Girolami et al. 2008).
- Rates of hindered settling are not influenced by shear (Girolami et al. 2008).
- Rates of hindered settling (deposition) decrease as a function of the degree of initial expansion of the flowing granular aggregate and are lower in fine aggregates than coarse aggregates (Girolami et al. 2008).
- After an initial phase of acceleration after release the flow fronts established a constant velocity that is a function of the initial height of release (square root of gh; Roche et al. 2008).
- Experimental granular flows deposit by progressive aggradation (Girolami et al. 2010; Roche et al. 2010).
- The flow front of experimental flows shears over the substrate, but behind the flow front, a no slip relationship exists between the flow and the aggrading depositional surface (Girolami et al. 2010).
- In experimental flows with a grain size <60 μm, air–particle viscous interactions can cause a fluid to have inertial, water-like, flow behaviour (Roche et al. 2008).
- Experimental air–particle granular flows can develop internal under-pressures in the flow front, but over-pressures in the body (Roche et al. 2010).

Numerical modelling studies have treated pyroclastic flows at either the scale of the entire flow, including the ash cloud (e.g. Valentine and Wohletz 1989; Giordano and Dobran 1994; Bursik and Woods 1996 and others) or have tried to simulate grain behaviour in granular flow parts of pyroclastic flows (e.g. Dufek and Bergantz 2007; Dufek et al. 2009). In simulations of whole flows, the volumetrically dominant low particle concentration ash cloud overwhelms the simulations, and little seems to be gleaned about the behaviour of the denser body under-flow, except that it exists and is susceptible to the effects of topographic impediments. Barranblatt (2009) has proposed that suspended particles in the spectrum of natural flows in which the fluid is a gas, including bush fires, lead to suppression of turbulence and the 'laminarization' of the basal part of the flow into a shearing style of flow that can become distinct from the over-riding more turbulent, but slower moving suspension part of the flow.

In simulations focussing on bed load or basal granular flow regions, Dufek and Bergantz (2007) noted that transport in granular bed load regions depend on momentum transfer between colliding grains rather that fluid–particle drag forces in the over-riding suspended transport regime. Dufek et al (2009) furthermore emphasise that in poly-disperse granular flow systems, for the larger grains to be transported significant distances, momentum transfer from the smaller grain population to the larger grain population must occur.

There are both temporal and spatial scaling problems in comparing the results of small-scale experimental flows with those of large-scale natural phenomena. Principal difficulties in making these comparisons are that the experimental flows to date have been essentially instantaneous lock release generated currents, not continuous feed currents, as is likely for large volume natural pyroclastic flows. Secondly, understanding what happens in a very hot, 50 to several hundred-metre-thick gas fluidised natural pyroclastic flow is totally different to what happens in a several centimetre-thick cold to hot, very small volume experimental flow. The thickness of the high particle concentration under-flow is totally unknown in natural flows, especially large volume flows, and also the nature of

the lateral transitions in the flow is totally unknown. Both will remain unknown until remote sensing techniques for imaging the internal physical properties of flows become more advanced. Nonetheless, the results of the experimental granular flows provide valuable insights into some of the processes that may occur in basal granular flow zones of natural pyroclastic flows.

In particular, processes that are consistent with our interpretations for the CGI flow system include the role of fine ash in a very thick flow in trapping gas and allowing the basal granular flow system to remain mobile for extended distances, the development of a basal laminar flow, shearing flow zone and likely progressive aggradation in at least proximal to medial flow domains.

Flow state of the CGI pyroclastic flow system

Pyroclastic flows are generally considered to be dynamic, variably turbulent flows of gas, ash, pumice and rock debris (Cas and Wright 1987; Druitt 1998; Branney and Kokelaar 2002). However, only the outer margins of the flows, including the flow front, marginal and trailing ash cloud, are clearly turbulent, based on historic observations, photography and film footage (e.g. Mount St. Helens, 1980, Rowley et al. 1981; Soufriere Hills, 1995–present; Loughlin et al. 2002). Our inability to see what happens inside the body of a pyroclastic flow limits our understanding of the flow dynamics of that part of a pyroclastic density current.

It is commonly recognized that the deposits of pyroclastic flows do not represent the physical flow state of the parent flow system (Branney and Kokelaar 2002). However, deposit characteristics are fundamental in reflecting many important dynamic aspects of pyroclastic flows, especially during deposition. Flow front and trailing/enclosing ash-cloud parts of flows produce distinctive deposit types (layers 1 and 3; Sparks et al. 1973; Fisher 1979; Wright et al. 1981; Cas and Wright 1987; Wohletz 2001), reflecting turbulence during transport and deposition. Layer 1 facies are poorly developed in the CGI.

The CGI consists overwhelmingly of the massive, poorly sorted layer 2 textured ignimbrite. It lacks continuous normal size grading, and the abundance of fine ash throughout the deposit indicates that sedimentation occurred from a thick basal high concentration part of the flow, not just a thin basal boundary layer. The sub-horizontal clast alignment fabric in the CGI, defined by large platy lithic and pumice clasts, but remarkably also by visible mineral grains, such as biotite, and the preserved sub-horizontal AMS fabric is interpreted to represent a laminar shear flow state in this thick basal granular flow. How much of the flow was flowing in such a laminar flow state is unclear, although given the ubiquitous sub-horizontal fabric, we believe a large part of the flowing mass was moving as a high particle concentration granular flow, which would have suppressed turbulence. No doubt there was a lower particle concentration more turbulent upper part, gradational into the ash cloud.

In comparison, the deposits of short-lived highly expanded, fully turbulent, subaqueous sedimentary turbidity currents are usually normal size-graded, unless they result from high particle concentration flows (Middleton 1993) or from sustained currents (e.g. Kneller and Branney 1995). Furthermore, highly turbulent, fully expanded, laterally flowing desert (Saharan) dust storms that carry micron-sized dust do not produce thick massive deposits that fill topography. They produce thin, mantling, fallout-like, dust layers (Tsoar and Pye 1987). The CGI flow system was nothing like these two flow types.

Although much ash can be elutriated from pyroclastic flows, especially through the enclosing, turbulent ash cloud, producing co-ignimbrite ash (e.g. Sparks et al. 1973; Cas and Wright 1987; Wohletz 2001), the abundance of a fine-ash matrix in layer 2 deposits of the CGI, as well as only minor crystal fragment enrichment in the matrix compared with the crystal content in the pumice fragments (i.e. only minor fine vitric ash elutriation from the eruption column and flow), is consistent with low levels of turbulence in the flow. In addition, the high emplacement temperature of the ignimbrite (Lesti et al. 2011) and the presence of welding in proximal to medial areas also support this interpretation.

Low aspect ratio of the CGI and factors contributing to it

Pyroclastic flow mobility or runout, reflected by aspect ratio, is likely to be a function of momentum, or velocity, which is influenced by the height of the source of the flow above the depositional area, the granulometry, particle concentration and the effectiveness of gas lubrication, the terrain and duration of the eruption and supply of pyroclastic debris and gas from the vent. The relative roles of these factors could change during a flow event and are obviously different for different flows and flow types. Although the CGI has a low aspect ratio, there is no evidence that the CGI flow system had a very high flow velocity (there is lack of basal erosional contacts, lack of coarse co-ignimbrite breccias and only minor occurrence of surges), as many LARIS-type flows may have experienced. The CGI therefore probably represents a relatively low velocity pyroclastic flow, and other factors must account for its low aspect ratio of 4.5×10^{-4}. We propose that gas fluidisation from gas trapped in the thick, voluminous, ash-rich, high particle concentration, granular under-flow of the CGI flow, was a key factor, likely promoted by a sustained mass flux. Secondly, high degrees of turbulence produced by high velocity flow would have led to gas loss and thus

loss of mobility, and so the flow was probably moving relatively slowly. Thirdly, the radially sloping, smooth low relief radial regional slope created by the previous Toconquis eruptive products and largely unimpeded by topographic obstacles can also create large runout distances, as demonstrated experimentally by Roche et al. (2005) and by numerical modelling (Dufek and Manga 2008). A prolonged constant, sustained discharge rate would also help to sustain a pyroclastic density current.

Eruption style for the CGI

As discussed by Folkes et al. (2011a), the absence of a plinian fall deposit beneath the CGI, the very minor enrichment of crystal fragments in the matrix compared with their abundance in the pumice clasts and the high emplacement temperature (Lesti et al. 2011) and development of welding in proximal to medial parts of the CGI indicate that the eruption column was never high and that it collapsed almost immediately the eruption began, so limiting the elutriation of vitric ash as well as limiting cooling of the pyroclasts in the column. The eruption was probably a low 'boiling over', fountain style eruption, with a relatively constant, sustained and high discharge rate. Since the CGI is represented by one massive depositional unit in most places, this suggests the eruption was continuous, with a constant, high mass flux. Similar characteristics for other very large volume, crystal-rich ignimbrites in the Andes suggest similar eruption styles for those ignimbrites as well.

The low level of vent-derived accessory lithic clasts indicates that the vent system was not created by just explosive excavation. Sparks et al. (1985) suggested the magma chamber roof block that foundered to produce the Cerro Galán Caldera, subsided along an outward dipping ring fracture, so enabling a more passive trans-tensional opening of the ring fracture vent system. This would have facilitated an immediate high magma discharge or eruption rate from the outset of the eruption. This would have caused instantaneous collapse of the developing eruption column, which would have transformed immediately into a continuously collapsing pyroclastic fountain and prevented fall deposits from forming.

Lack of evidence of erosional interaction between the CGI and the substrate?

There is a remarkable lack of evidence for erosional interaction between the base of the CGI and the substrate because scours are rare, and accidental lithics are minor, are small and do not appear to have been transported far. The CGI pyroclastic flow therefore did not exert a significant horizontal shear force on the substrate over which it moved. This is intuitively surprising, given how dynamic pyroclastic flows are commonly depicted as being. Although this is explained in existing models by the existence of inert basal depositional boundary layers (e.g. Fisher 1966), we have no indication that such boundary layers would be significant in very thick, low turbulence flow systems. Given that pyroclastic flows contain high trapped hot gas content, they develop a high internal gas over-pressure (Sparks 1976; Wilson 1985) because hot interstitial gas is expanding. Non-erosional contacts can thus be explained by a downward directed gas pressure from within the flow, acting downwards onto the ground surface. This would reduce the coefficient of friction between the base of the flow and the substrate, allowing the pyroclastic flows to virtually glide over the ground surface. Although this may have occurred with the CGI, clearly some flows are capable of exerting significant erosional force on the substrate, at least locally (e.g. Taupo ignimbrite, Wilson 1985).

Conclusions

1. The Cerro Galán Ignimbrite is an amazingly uniform deposit given its >630 km^3 volume and the terrain over which the parent pyroclastic flow system travelled.
2. The ignimbrite is most commonly represented by a single massive depositional unit. Only at distal margins where the flow system travelled through irregular palaeotopography are multiple depositional units preserved, separated by very thin centimetres thick ash-cloud surge deposits, or trails of locally derived basement lithic clasts, or concentrations of pumice clasts. It appears the topography induced some degree of turbulence and the development of unsteadiness of flow competence and capacity, resulting in multiple depositional pulses.
3. At least away from the vent area, however, turbulence was suppressed because depositional units and their boundaries are horizontal in palaeovalleys, units onlap palaeovalley walls and palaeoflow indicators (e.g. AMS fabrics, clast imbrication, mineral alignment) almost always indicate flow sub-parallel to palaeovalley axes.
4. Furthermore, where the CGI has in-filled palaeovalleys and then been deposited on inter-fluve palaeoridges, the facies are also massive, and not typical, stratified ignimbrite veneer facies, again suggesting a lack of significant turbulence.
5. Lithic clast content is generally low (<3%) and consists mostly of small local, basement-derived accidental lithics. In most cases, these have not been

transported far from their source point. Where large basement pelite clasts occur, they are often disaggregated into a jigsaw fit cluster of small slices of the large clast. Such clusters indicate very limited transport distances and very limited levels of turbulence; otherwise, those clusters would be dispersed randomly throughout the ignimbrite.

6. An almost pervasive sub-horizontal fabric of aligned elongate lithic and pumice clasts and even biotite and feldspar crystals in the ignimbrite matrix, at all levels in the ignimbrite, even where it is non-welded, indicates the existence of a strong horizontal shear force throughout the depositional system. We interpret this is being due to a laminar flow regime in a high particle concentration, shearing, granular pyroclastic flow system. The presence of abundant ash matrix in the massive deposit (>80% of the deposit is ash) is also consistent with a high particle concentration granular flow regime with suppressed turbulence or non-turbulent laminar flow regime in the body of the deposit. Such a non-turbulent flow regime would limit significant ash elutriation.
7. A high particle concentration, poly-disperse granular flow would cause gas to be trapped, leading to fluidisation induced flow mobility of the pyroclastic flow. High velocities to account for flow distances of up to 100 km and a low aspect ratio for the CGI are not necessary.
8. The generally non-erosive deposit base, the rare occurrence of layer 1 deposits, the lithic-poor nature of the ignimbrite and the local derivation of basement accidental lithic clasts are also consistent with a relatively low flow velocity. The combination of low flow velocity, high particle concentration and high bulk flow density would have the effect of suppressing turbulence.
9. Calculations of the likely force required to move the largest accidental substrate lithic clasts, the dynamic pressure generated and the likely flow velocity are surprisingly low, with values of 151 N, 4.7 kPa and< 3 ms^{-1} (<10 km h^{-1}), respectively, are surprisingly low compared with other documented pyroclastic flows. This is explained as being due to low eruption column height (collapsing fountain) and gently sloping, radial, planar substrate surface over which the flow system largely flowed.
10. Surprisingly also, the aspect ratio of the CGI deposit is low (LARI). Although LARI-type ignimbrites have previously been attributed to very high velocity flow regimes, we interpret the low aspect ratio nature of the CGI as resulting from sustained eruption of a large volume of fine pyroclastic debris and flow radially down a gently sloping and relatively flat surface produced by previous large volume eruptions that built a gently sloping (8–9°) ignimbrite shield.
11. The relatively rare occurrence of erosional bases for pyroclastic flow deposits can be explained by an internal, gas over-pressure directed downwards onto the substrate over which the flow moves. This would significantly lower the coefficient of friction between the base of the flow and the substrate and could even produce a pressurised gas cushion at the base of the pyroclastic flow over which the body largely glides. Occasional occurrences of erosional interaction indicate frictional coupling between the flow and the substrate, leading to shearing and erosion and reflecting both significant levels of turbulence and velocity.

Acknowledgements We thank the Australian Research Council Discovery Grant Scheme for funding most of the costs of this research through grant DP0663560 to undertake research on the volcanology of the Cerro Galán ignimbrite. Careful reviews by Greg Valentine and Tim Druitt and very helpful editorial suggestions by Kathy Cashman and James White have greatly improved the paper.

References

Allen SR, Cas RAF (1998) Lateral variations within coarse co-ignimbrite lithic breccias of the Kos Plateau Tuff, Greece. Bull Volcanol 59:356–377

Allen SR, Cas RAF (2001) Transport of pyroclastic flows across the sea during the explosive, rhyolitic eruption of the Kos Plateau Tuff, Greece. Bull Volcanol 62:441–456

Barranblatt GI (2009) Shear flow laminarization and acceleration by suspended heavy particles: a mathematical model and geophysical applications. Comm Appl Math Comp Sci 4:153–175

Branney MJ, Kokelaar BP (2002) Pyroclastic density currents and the sedimentation of ignimbrites. Geol Soc London Mem 27:152

Buesch D (1992) Incorporation and redistribution of locally derived lithic fragments within a pyroclastic flow. Geol Soc Am Bull 104:1193–1207

Bursik M, Woods A (1996) The dynamics and thermodynamics of large ash flows. Bull Volcanol 58:175–193. doi:10.1007/s004450050134

Cas RAF, Wright JV (1987) Volcanic successions, modern and ancient. Allen and Unwin, London, 527 pp

Chadima M, Jelinek V (2009) Anisoft 4.2—Anisotropy data browser

De Silva SL (1989) Geochronology and stratigraphy of the ignimbrites from the 21°30′S to 23°30′S portion of the central Andes of northern Chile. J Volcanol Geotherm Res 37:93–131

Dellino P, Zimanowski B, Buttner R, La Volpe L, Mele D, Sulpizio R (2007) Large-scale experiments on the mechanics of pyroclastic flows: design, engineering, and final results. J Geophys Res 112: B04202. doi:10.1029/2006JB004313

Druitt TH (1998) Pyroclastic density currents. In: Gilbert JS, Sparks RSJ (eds) The physics of explosive eruptions. Geol Soc London Spec Pub 145. Geological Society of London, London, pp 145–182

Druitt TH, Avard G, Bruni G, Lettieri P, Maes F (2007) Gas retention in fine-grained pyroclastic flow materials at high temperatures. Bull Volcanol 69:881–901

Dufek J, Bergantz GW (2007) Suspended load and bed-load transport of particle-laden gravity currents: the role of particle–bed interaction. Theor Comput Fluid Dyn. doi:10.1007/s00162-007-0041-6

Dufek J, Manga M (2008) In situ production of ash in pyroclastic flows. J Geophys Res 113:B09207. doi:10.1029/2007JB00555

Dufek J, Wexler J, Manga M (2009) Transport capacity of pyroclastic density currents: experiments and models of substrate-flow interaction. J Geophys Res 114:B11203–B11215. doi:10.1029/2008JB006216

Esposti Ongaro T, Widiwijayanti C, Clarke AB, Voight B, Neri A (2011) Multiphase-flow numerical modeling of the 18 May 1980 lateral blast at Mount St. Helens, USA. Geology 39:535–538

Fisher RV (1966) Mechanism of deposition from pyroclastic flows. Am J Sci 264:350–363

Fisher RV (1979) Models for pyroclastic surges and pyroclastic flows. J Volcanol Geotherm Res 6:305–318

Fisher RV (1990) Transport and deposition of a pyroclastic surge across an area of high relief: the 18 May 1980 eruption of Mount St. Helens. Washington Bull Geol Soc Am 102:1038–1054

Fisher RV, Orsi G, Ort M, Heiken G (1993) Mobility of a large-volume pyroclastic flow—emplacement of the Campanian ignimbrite, Italy. J Volcanol Geotherm Res 56–3:205–220

Folkes CB, Wright HM, Cas RAF, de Silva SL, Lesti C, Viramonte JG (2011a) A re-appraisal of the stratigraphy and volcanology of the Cerro Galán volcanic system, NW Argentina. In: Cas RAF, Cashman K (eds) The Cerro Galan Ignimbrite and Caldera: characteristics and origins of a very large volume ignimbrite and its magma system. Bull Volcanol. doi:10.1007/s00445-011-0459-y

Folkes CB, de Silva S, Wright HM, Cas RAF (2011b) Geochemical homogeneity of a long-lived large silicic system: evidence from Cerro Galan Caldera, NW Argentina. In: Cas RAF, Cashman K (eds) The Cerro Galan Ignimbrite and Caldera: characteristics and origins of a very large volume ignimbrite and its magma system. Bull Volcanol. doi:10.1007/s00445-011-0511-y

Francis PW, Hammill M, Kretzschmar G, Thorpe RS (1978) The Cerro Galán Caldera, NW Argentina and its tectonic setting. Nature 274:749–751

Francis PW, O'Callaghan L, Kretzschmar GA, Thorpe RS, Sparks RSJ, Page RN, de Barrio RE, Gillou G, Gonzalez OE (1983) The Cerro Galán Ignimbrite. Nature 301:51–53

Francis PW, Sparks RSJ, Hawkesworth CJ, Thorpe RSJ, Pyle DM, Tait SR, Mantovani MS, McDermott F (1989) Petrology and geochemistry of volcanic rocks of the Cerro Galán Caldera, northwest Argentina. Geol Mag 126:515–547

Freundt A, Schmincke H-U (1986) Emplacement of small-volume pyroclastic flows at Laacher See (East-Eifel, Germany). Bull Volcanol 48:39–59

Giordano G (1998) The effect of paleo-topography on lithic distribution and facies associations of small volume ignimbrites: an insight into transport and depositional systems of WTT Cupa deposits (Roccamonfina volcano, Italy). J Volcanol Geotherm Res 87:255–273

Giordano G, Dobran F (1994) Computer simulations of the Tuscolano Artemisios 2nd Pyroclastic Flow Unit (Alban Hills, Latium, Italy). J Volcanol Geotherm Res 61:69–94

Giordano G, De Rita D, Cas RAF, Rodani S (2002) Valley pond and ignimbrite veneer deposits in small volume phreatomagmatic basic ignimbrite, Lago Albano Maar, Colli Albani volcano, Italy: influence of topography. J Volcanol Geotherm Res 118:131–144

Girolami L, Druitt TH, Roche O, Khrabrykh Z (2008) Propagation and hindered settling of laboratory ash flows. J Geophys Res 113:B02202

Girolami L, RocheO DTH, Corpetti T (2010) Particle velocity fields and depositional processes in laboratory ash flows, with implications for the sedimentation of dense pyroclastic flows. Bull Volcanol 72:747–759

Hildreth W (1983) The compositionally zoned eruption of 1912 in the Valley of Ten Thousand Smokes, Katmai National Park, Alaska. J Volcanol Geotherm Res 18:1–18

Hongn FD, Seggiaro RE (2001) Hoja Geológica 2566-III, Cachi. Provincias de Salta y Catamarca, Programa Nacional de Cartas Geológicas de la República Argentina. SEGEMAR, Buenos Aires, p 87

Jelinek V (1978) Statistical processing of anisotropy of magnetic susceptibility measures on groups of specimens. Studia Geophis Geodet 22:50–62

Kay SM, Coira B, Wörner G, Kay RW, Singer BS (2011) Geochemical, isotopic and single crystal $^{40}Ar/^{39}Ar$ age constraints on the evolution of the Cerro Galán Ignimbrites. In: Cas RAF, Cashman K (eds) The Cerro Galan Ignimbrite and Caldera: characteristics and origins of a very large volume ignimbrite and its magma system. Bull Volcanol. doi:10.1007/s00445-010-0410-7

Kieffer SW, Sturtevant B (1988) Erosional furrows formed during the lateral blast at Mount St. Helens, May 18, 1980. J Geophys Res 93:14,793–14,816

Kneller BC, Branney MJ (1995) Sustained high-density turbidity currents and the deposition of thick massive sands. Sedimentology 42:607–616

Knight MD, Walker GPL, Ellwood BB, Diehl JF (1986) Stratigraphy, paleomagnetism, and magnetic fabric of the Toba Tuffs: constraints on their sources and eruptive styles. J Geophys Res 91:10, 355–10, 382

Lesti C (2010) Emplacement temperature and flow direction analysis of large dimension calderas ignimbrites: the Cerro Galán and Toconquis Group ignimbrites (Puna plateau, NW Argentina). Ph. D. thesis, Universita di Roma Tre, Italy 97 pp

Lesti C, Porreca M, Giordano G, Mattei M, Cas R, Wright H, Viramonte J (2011) High temperature emplacement of the Cerro Galán and Toconquis Group ignimbrites (Puna plateau, NW Argentina) determined by TRM analyses. In: Cas RAF, Cashman K (eds) The Cerro Galan Ignimbrite and Caldera: characteristics and origins of a very large volume ignimbrite and its magma system. Bull Volcanol. doi:10.1007/s00445-011-0536-2

Lindsay JM, de Silva SL, Trumbull R, Emmermann R, Wemmer R (2001) La Pacana caldera, N. Chile: a re-evaluation of the stratigraphy and volcanology of one of the world's largest resurgent calderas. J Volcanol Geotherm Res 106:145–173

Loughlin SC, Calder ES, Clarke A, Cole PD, Luckett R, Mangan MT, Pyle DM, Sparks RSJ, Voight B, Watts RB (2002) Pyroclastic flows and surges generated by the 25 June 1997 dome collapse, Soufriere Hills Volcano, Montserrat. In: Druitt TH, Kokelaar BP (eds) The eruption of Soufriere Hills Volcano, Monstserrat, from 1995 to 1999. Geol Soc London Mem 21. Geological Society of London, London, pp 191–210

Middleton GV (1993) Sedimentation from turbidity currents. Ann Rev Earth Planet Sci 29:89–114

Nakada S, Fujii T (1993) Preliminary report on the activity at Unzen Volcano (Japan), November 1990–November 1991: dacite lava domes and pyroclastic flows. J Volcanol Geotherm Res 54:319–333

Ort MH (1993) Eruptive processes and caldera formation in a nested downsagcollapse caldera: Cerro Panizos, central Andes Mountains. J Volcanol Geotherm Res 56:221–252

Ort MH, Orsi G, Pappalardo L, Fisher RV (2003) Anisotropy of magnetic susceptibility studies of depositional processes in the Campanian Ignimbrite, Italy. Bull Volcanol 65:55–72

Pittari A, Cas RAF, Edgar C, Nichols H, Wolff JA, Marti J (2006) The influence of palaeotopography on facies architecture and pyroclastic flow processes of a lithic-rich ignimbrite in a high gradient setting: the Abrigo Ignimbrite, Tenerife, Canary Islands. J Volcanol Geotherm Res 152:273–315

Pittari A, Cas RAF, Monaghan J, Marti J (2007) Instantaneous dynamic pressure effects on the behaviour of lithic boulders in pyroclastic flows: the Abrigo Ignimbrite, Tenerife, Canary Islands. Bull Volcanol 69:265–279

Quane SL, Russell JK (2005) Ranking welding intensity in pyroclastic deposits. Bull Volcanol 67:129–143

Roche O, Gilbertson MA, Philips JC, Sparks RSJ (2005) Inviscid behaviour of fines-rich pyroclastic flows inferred from experiments on gas–particle mixtures. Earth Planet Sci Lett 240:401–414

Roche O, Gilbertson MA, Philips JC, Sparks RSJ (2006) The influence of particle size on the flow of initially fluidised powders. Powder Technol 166:167–174. doi:10.1016/j.powtec.2006.05.010

Roche O, Montserrat S, Nino Y, Tamburrino A (2008) Experimental observations of water-like behavior of initially fluidized dam break granular flows and their relevance for the propagation of ash-rich pyroclastic flows. J Geophys Res 113:B12203. doi:10.1029/2008JB005664

Roche O, Montserrat S, Nino Y, Tamburrino A (2010) Pore fluid pressure and internal kinematics of gravitational laboratory air–particle flows: insights into the emplacement dynamics of pyroclastic flows. J Geophys Res 115:B09206. doi:10.1029/2009JB007133

Rosi M, Vezzoli L, Aleotti P, De Sensi M (1996) Interaction between caldera collapse and eruptive dynamics during the Campanian Ignimbrite eruption, Phlegrean Fields, Italy. Bull Volcanol 57:541–554

Rowley PD, Kuntz MA, MacLeod NS (1981) Pyroclastic flow deposits. In: Lipman PW, Mullineaux DR (eds) The 1980 eruptions of Mount St. Helens, Washington. US Geol Surv Prof Pap 1250:489–512

Schumacher R, Mues-Schumacher U (1996) The Kizilkaya ignimbrite—an unusual low-aspect-ratio ignimbrite from Cappadocia, central Turkey. J Volcanol Geotherm Res 70:107–121

Scott WE, Hoblitt RP, Torres RC, Self S, Martinez MML, Nillos T (1996) Pyroclastic flows of the June 15, 1991, climactic eruption of Mount Pinatubo. In: Newhall CG, Punongbayan RS (eds) Fire and mud; eruptions and lahars of Mount Pinatubo. University of Washington Press, Seattle, Philippines, pp 545–570

Self S, Goff F, Gardner JN, Wright JV, Kite WM (1986) Explosive rhyolitic volcanism in the Jemez Mountains: vent locations caldera development and relation to regional structure. J Geophys Res 91:1779–1798

Smith RL, Bailey RA (1966) The Bandelier Tuff: a study of ash-flow eruption cycles from zoned magma chambers. Bull Volcanol 29:83–103

Sparks RSJ (1976) Grain size variations in ignimbrites and implications for transport of pyroclastic flows. Sedimentology 23:147–188

Sparks RSJ, Self S, Walker GPL (1973) Products of ignimbrite eruptions. Geology 1:115–118

Sparks RSJ, Francis PW, Hamer RD, Pankhurst RJ, O'Callaghan LO, Thorpe RS, Page R (1985) Ignimbrites of the Cerro Galán Caldera, NW Argentina. J Volcanol Geotherm Res 24:205–248

Stern CR (2004) Active Andean volcanism: its geologic and tectonic setting. Revista Geol Chile 31:161–206

Tsoar H, Pye K (1987) Dust transport and the question of desert loess formation. Sedimentology 34:139–153

Valentine GA (1998) Damage to structures by pyroclastic flows and surges, inferred from nuclear weapons effects. J Volcanol Geotherm Res 87:117–140

Valentine GA, Wohletz KH (1989) Numerical models of Plinian eruption columns and pyroclastic flows. J Geophys Res 94:1867–1887. doi:10.1029/JB094iB02p01867

Viramonte JG, Galliski MA, Saavedra V, Aparicio A, García Cacho L, Escorza M (1984) El finivulcanismo básico de la Depresión de Arizaro, provincia de Salta, República Argentina. IX Congreso Geológico Argentino, Actas III: 234–254

Walker GPL (1983) Ignimbrite types and ignimbrite problems. J Volcanol Geotherm Res 17:281–296

Walker GPL, Hemming RF, Wilson CJN (1980) Low aspect ratio ignimbrites. Nature 283:286–287

Walker GPL, Wilson CJN, Frogatt PC (1981) An ignimbrite veneer deposit: the trail-marker of a pyroclastic flow. J Volcanol Geotherm Res 9:409–421

Watkins SD, Giordano G, Cas RAF, De Rita D (2002) Emplacement processes of the mafic Villa Senni Eruption Unit (VSEU) ignimbrite succession, Colli Albani volcano, Italy. In: Cas RAF, Wildner W (eds) Volcanic and associated regimes—the complexity of volcanic systems. J Volc Geotherm Res 118, pp 173–203

Wilson CJN (1985) The Taupo eruption, New Zealand. II. The Taupo ignimbrite. Philos Trans R Soc Lond A 314:229–310

Wilson CJN (2001) The 26.5 ka Oruanui eruption, New Zealand: an introduction and overview. J Volcanol Geotherm Res 112:133–174

Wilson CJN, Hildreth WE (1997) The Bishop Tuff: new insights from eruptive stratigraphy. J Geol 105:407–439

Wilson CJN, Hildreth WE (2003) Assembling an ignimbrite: mechanical and thermal building blocks in the Bishop Tuff, California. J Geol 111:653–670

Wilson CJN, Walker GPL (1985) The Taupo eruption, New Zealand I. General aspects. Philos Trans R Soc Lond A 314:199–228

Wohletz KH (2001) Pyroclastic surges and compressible two-phase flow. In: Freundt A, Rosi M (eds) From magma to tephra. Developments in volcanology 4. Elsevier, Amsterdam, pp 247–312

Woods AV, Bursik MI, Kurbatov AV (1998) The interaction between ash flows and ridges. Bull Volcanol 60:38–51

Wright JV, Self S, Fisher RV (1981) Towards a facies model for ignimbrite-forming eruptions. In: Self S, Sparks RSJ (eds) Tephra studies. Reidel, Dordrecht, pp 433–439

Wright HMN, Folkes CB, Cas RAF, Cashman KV (2011a) Heterogeneous pumice populations in the 2.08 Ma Cerro Galán ignimbrite: implications for magma recharge and ascent preceding a large volume silicic eruption. In: Cas RAF, Cashman K (eds) The Cerro Galan Ignimbrite and Caldera: characteristics and origins of a very large volume ignimbrite and its magma system. Bull Volcanol. doi:10.1007/s00445-011-0525-5

Wright HMN, Lesti C, Cas RAF, Porecca M, Viramonte J, Folkes CB, Giordano G. (2011b) Columnar jointing in vapor phase altered, non-welded Cerro Galan Ignimbrite, Paycuqui, Argentina. In: Cas RAF, Cashman K (eds) The Cerro Galan Ignimbrite and Caldera: characteristics and origins of a very large volume ignimbrite and its magma system. Bull Volcanol. doi:10.1007/s00445-011-0524-6

Yamamoto T, Takarada S, Suto S (1993) Pyroclastic flows from the 1991 eruption of Unzen volcano, Japan. Bull Volcanol 55:166–175